Kinetics and Mechanism of the Lamellar Gel/Lamellar Liquid-Crystal and Lamellar/Inverted Hexagonal Phase Transition in Phosphatidylethanolamine: A Real-Time X-ray Diffraction Study Using Synchrotron Radiation†

Martin Caffrey

Section of Biochemistry, Molecular and Cell Biology, Division of Biological Sciences, Cornell University, Ithaca, New York 14853

Received December 18, 1984; Revised Manuscript Received March 25, 1985

ABSTRACT: A study of the kinetics and mechanism of the thermotropic lamellar gel/lamellar liquid-crystalline and lamellar/inverted hexagonal phase transition in dihexadecylphosphatidylethanolamine (DHPE) at various hydration levels has been carried out. Measurements were made by using a real-time X-ray diffraction method at the Cornell High Energy Synchrotron Source. This represents an extension of an earlier study concerning the lamellar gel/lamellar liquid-crystalline phase transition in dipalmitoylphosphatidylcholine [Caffrey, M., & Bilderback, D. H. (1984) *Biophys. J. 45*, 627–631]. With DHPE, the chain-melting and the nonbilayer transitions were examined under active heating and passive cooling conditions by using a temperature jump to effect phase transformation. Measurements were made at hydration levels ranging from 0% to 60% (w/w) water, and in all cases, the transitions were found to (1) be repeatable, (2) be reversible, and (3) have an *upper bound* on the transit times (time required to complete the transition) of ≤ 3 s. The shortest transit time recorded for the chain-melting and lamellar/hexagonal transitions was <1 s. At 8% (w/w) water, the transit times were still on the order of seconds even though the transition does not involve the intermediate L_α phase. *Note*, the measured transit times are gross values incorporating the intrinsic transit time in addition to the time required to heat or cool the sample through the transition temperature range and to supply or remove the latent heat of the transition. Regardless of the direction of the transition, both appear to be two state to within the sensitivity limits of the real-time method. From simultaneous wide- and low-angle measurements at the lamellar chain-melting transition, loss of long-range order in the lamellar gel phase appears to precede the chain-melting process. On the basis of the real-time X-ray diffraction measurements, a mechanism is proposed for the lamellar/hexagonal phase transition. The mechanism (1) does not involve large or energetically expensive molecular rearrangements, (2) leads directly to a hexagonal lattice coplanar with the lamellar phase, (3) incorporates facile reversibility, repeatability, and cooperativity, (4) accounts for an observed, apparent memory in the hexagonal phase of the original lamellar phase orientation, and (5) is consistent with the experimental observation of a predominantly two-state transition. In conjunction with the kinetic measurements, the DHPE/water phase diagram was constructed. At and above 12% (w/w) water, the thermotropic transition sequence is $L_{\beta'}/L_\alpha/H_{II}$. Below this hydration level, the transition involves a direct $L_{\beta'}/H_{II}$ conversion without the intermediate L_α phase. The lamellar gel phase is metastable, is of the $L_{\beta'}$ (tilted chain) type, and has a maximum water content of 16% (w/w). Structural parameters of the $L_{\beta'}$ phase and thermal expansivity of the long spacing for the three phases are reported.

The bimolecular lipid membrane is the fundamental structural component and permeability barrier of biological membranes. Pure lipids have provided useful models for studying membrane lipid components in isolation, in mixtures with other lipid species, and in reconstituted systems with membrane proteins and other molecules. Many biological and synthetic lipids when fully hydrated exist in the lamellar phase. Here lipid bilayers stack on top of one another separated by a layer of water whose thickness varies with lipid head-group type and with charge in and on the membrane (Luzzati, 1968; Shipley, 1973).

The lamellar phase is periodic in one dimension. At low temperatures, the acyl chains adopt a close-packed hexagonal or quasi-hexagonal arrangement. The chains are fully extended in all all-trans conformation with rotational motion about the long axis of the molecule (Marsh, 1980). In this so-called gel phase, chains may be tilted ($L_{\beta'}$) or untilted (L_β) with respect to the bilayer normal (Tardieu et al., 1973; Ranck et al., 1974), and lateral motion in the plane of the membrane is slow (Wu et al., 1977; Fahey & Webb, 1978). The L_β and $L_{\beta'}$ phases may represent metastable polymorphs which give rise to a more stable phase (L_C) wherein the acyl chains are packed in a very highly ordered almost crystalline manner (Chen et al., 1980; Cameron & Mantsch, 1982; Ruocco & Shipley, 1982a). Above the chain-melting transition temperature, the acyl chains undergo extensive trans/gauche isomerization reminiscent of a fluid hydrocarbon. This is the lamellar liquid-crystal phase (L_α) and is characterized by rapid translational motion in the membrane plane and by considerable, although incomplete, short-range disorder (Luzzati, 1968).

Another lipid phase which of late has received considerable attention is the inverted hexagonal (H_{II}) phase (Luzzati, 1968). This phase is periodic in two dimensions and is considered one of the nonbilayer phases. It consists of hexagonally packed water cylinders of indefinite length with an outer lining of lipid molecules oriented with acyl chains facing radially away from the cylinder axis and with the head groups buried in the inner aqueous channel.

† This work was supported by a grant from the National Institutes of Health, U.S. Public Health Service (HL-18255), to G. W. Feigenson.

0006-2960/85/0424-4826$01.50/0

Interest in the inverted hexagonal phase arises because (1) many naturally derived lipids including phosphatidylethanolamine (PE),[1] phosphatidic acid (PA), phosphatidylglycerol (PG), cardiolipin (CL), monoacyl glycerides (MG), diacyl glycerides (DG), monogalactosyl diglyceride (MGDG), and monoglucosyl diglyceride (MGluDG) can form or induce formation of this phase when hydrated under physiological conditions (Rand & Sengupta, 1972; Shipley et al., 1973; Larsson et al., 1980; Harlos & Eibl, 1980, 1981; Chang & Yager, 1983; Sprague & Staehelin, 1983; Das & Rand, 1984; Dea et al., 1985; Eibl, 1984; Miner & Prestegard, 1984), (2) from a topological perspective vital cellular processes such as membrane fusion must involve, if only locally and transiently, nonbilayer intermediates, (3) evidence primarily from X-ray diffraction, ^{31}P NMR, and freeze–fracture electron microscopy has been obtained for the existence of a H_{II} phase in biologically derived lipids and in isolated membrane preparations usually under conditions of reduced water activity (Deamer et al., 1970; Rand & Sengupta, 1972; Cullis & DeKruijff, 1979; Cullis et al., 1980; Corless & Costello, 1981; Hui et al., 1981a,b, 1983; Van Echteld et al., 1981; DeKruijff et al., 1982; Crowe & Crowe, 1982; Gruner et al., 1982; Boni & Hui, 1983; Gounaris et al., 1983; Platt-Aloia et al., 1983; Dea et al., 1985; Gordon-Kamm & Steponkus, 1984; Gulik-Krzywicki et al., 1984; Mollevanger & DeGrip, 1984; Verkleij, 1984), (4) the H_{II} phase can be triggered ionotropically on a result either of direct binding to a particular lipid species or of a metal ion induced phase separation (Rand & Sengupta, 1972; Cullis & DeKruijff, 1979; Harlos & Eibl, 1980, 1981; Van Venetie & Verkleij, 1981; DeKruijff et al., 1982; Verkleij et al., 1982; Miner & Prestegard, 1984; Tilcock et al., 1984), and (5) the activity of membrane-associated enzymes is influenced by lipids which can form the inverted hexagonal phase (Hui et al., 1981a,b; Jensen & Schutzbach, 1984; Navarro et al., 1984; Grunner, 1985). Furthermore, structures reminiscent of the individual lipid-coated water cylinders that make up the H_{II} phase have been implicated in such membrane functions as (1) transbilayer lipid movement (Cullis & DeKruijff, 1979; Corless & Costello, 1981; Noordam et al., 1981), (2) visual transduction (Albert et al., 1984; Mollevanger & DeGrip, 1984), (3) membrane-mediated transport (Cullis & DeKruijff, 1979; Cullis et al., 1980), and (4) membrane fusion (Cullis & DeKruijff, 1979; Cullis et al., 1980; Hui et al., 1981a,b). They have also been suggested to be intermediates in the lamellar/hexagonal phase transition (Verkleij et al., 1980; Hui et al., 1983; Seigel, 1984) and may constitute the tight junction strands between epithelial cells (Kachar & Reese, 1982; Meyer, 1983).

In cases where a hexagonal-like phase has been seen in biological membranes, phase separation of lipid species and protein clearing appear to accompany the nonbilayer transformation (Corless & Costello, 1981; Gordon-Kamm & Steponkus, 1984). However, it should be noted that in certain circumstances nonlipid components such as the model membrane protein gramicidin can be an integral part of the hexagonal phase (Van Echteld et al., 1981, 1982).

A substantial amount of information has been gathered on the equilibrium properties of the lamellar and to a lesser extent the hexagonal phase. However, details of the kinetics and the mechanism of these transitions are scant. In the recent past, a number of reports have appeared addressing these and related lipid phase transitions. The methods used to follow the transition kinetics include X-ray diffraction (Dupont et al., 1972; Dafler, 1977; Akiyama, 1981; Akiyama et al., 1982; Ruocco & Shipley, 1982b; Ranck, 1983; Caffrey & Bilderback, 1983, 1984; Caffrey, 1984; Persson, 1984; Ranck et al., 1984), Raman scattering (Yager & Peticolas, 1982), calorimetry (Cho et al., 1981; Johnson et al., 1983), dilatometry (Nagle & Wilkinson, 1982), ultrasonic relaxation (Eggers & Funck, 1976; Mitaku et al., 1978, 1983; Sano et al., 1982), and absorbance (Owen et al., 1970; Hammes & Tallman, 1970; Tsong, 1974; Clegg & Elson, 1975; Tsong & Kanehisa, 1977; Gruenewald et al., 1980, 1981; Holzwarth et al., 1982; Elamrani & Blume, 1983, 1984; Eck & Holzwarth, 1984), and fluorescence spectroscopy (Inoue et al., 1981; Lentz et al., 1978; Strehlow & Jahnig, 1981). A real-time X-ray diffraction method has recently been developed at the Cornell High Energy Synchrotron Source (CHESS) to study, among other things, the kinetics and mechanism of lipid phase transitions (Caffrey & Bilderback, 1983, 1984; Caffrey, 1984). The first transition to be examined by using the real-time method was the thermotropic chain melting in the lamellar phase of DPPC (Caffrey & Bilderback, 1983, 1984). The transit time from the lamellar gel to the lamellar liquid-crystal phase was measured at $\leq$2s, and the transition was between two states with no detectable intermediates to within the sensitivity limits of the method. In the present paper, these real-time measurements have been extended to include an investigation of the kinetics and mechanism of the thermotropic lamellar gel/lamellar liquid-crystal and lamellar/hexagonal phase transitions of phosphatidylethanolamine. The particular lipid used in the study was dihexadecylphosphatidylethanolamine (DHPE), and the transitions were studied in both the heating and cooling directions. The results show that, regardless of the direction and degree of hydration and despite the changes in periodicity and in long- and short-range order, all transitions occurred with transit times (time required to complete the transition) of <3 s. On the basis of these findings, a mechanism is proposed for the lamellar/hexagonal transition which is readily reversible, does not involve large molecular or energetically expensive rearrangements, naturally sets up a coplanar hexagonal lattice, and propagates from the nucleation site in all directions throughout the sample. In addition, the empirical phase diagram for DHPE/water and structural parameters of some of the low-temperature DHPE phases are presented.

Experimental Procedures

Materials. DHPE, obtained from Fluka Chemical Corp. (Hauppauge, NY), had a purity of ≥98% as judged by thin-layer chromatography of 100 μg of lipid in three solvent systems (acid, neutral, and basic) each on two solid supports

[1] Abbreviations: CHESS, Cornell High Energy Synchrotron Source; CESR, Cornell Electron–Positron Storage Ring; DHPE, dihexadecylphosphatidylethanolamine; DPPC, dipalmitoylphosphatidylcholine; PC, phosphatidylcholine; PA, phosphatidic acid; CL, cardiolipin; MGDG, monogalactosyl diglyceride; MGluDG, monoglucosyl diglyceride; NMR, nuclear magnetic resonance; EPR, electron paramagnetic resonance; TLC, thin-layer chromatography; GeV, billion electron volts; keV, thousand electron volts; d, lamellar spacing; d_w, water layer thickness; d_l, lipid bilayer thickness; S, interfacial surface area per lipid molecule; S_c, acyl chain cross-sectional area; α, thermal diffusivity; h, convective heat transfer coefficient; k, thermal conductivity; C_p, heat capacity; ν, kinematic viscosity; Pr, Prandtl number; Re, Reynolds number; U_∞, air stream velocity; $T(r,\tau)$, sample temperature at position r and elapsed time τ; T_∞, air stream temperature; T_0, initial sample temperature; ρ, density; μ, dynamic viscosity; C and n, constants; r, radial position in the capillary; r_0, capillary radius; τ, time; K, equilibrium constant of a pseudounimolecular reaction; ΔH_{cal}, calorimetrically determined enthalpy change; γ, degree of transition; FWHM, full width at half-maximum peak height; PE, phosphatidylethanolamine; PG, phosphatidylglycerol; MG, monoacyl glyceride(s); DG, diacyl glyceride(s); DDPE, didodecylphosphatidylethanolamine; lipid phase notation used is that of Luzzati (1968).

(Whatman K5F silica gel, Whatman; Adsorbosil 5-P plates, Applied Science) as previously described (Caffrey & Feigenson, 1981) and was used without further purification. Water was obtained from a Milli-Q water purification system (Millipore). All other chemicals and solvents were of reagent grade.

Sample Preparation. The dry powdered DHPE was finely chopped with a razor blade on a glass plate, transferred to preweighed, thin-walled (10-μm) glass capillaries (1-mm internal diameter, Supper), tapped to the bottom of the capillary, and reweighed. The actual capillary diameter was measured 1 cm from the tip of the capillary by using a light microscope with a micrometer ocular at 1.04 ± 0.10 mm (n = 25). Sample sizes varied from 5 to 10 mg per capillary, and weighings were to the nearest 0.05 mg with an accuracy of ±0.1 mg. To minimize the effect of weighing and volume measurement errors, the larger samples were used in preparing samples with the lowest hydration levels. Water was added to the top of the capillary by using a microsyringe and was immediately spun into the lipid powder by centrifugation at maximum speed in a swinging-bucket rotor (International Clinical centrifuge, Model 1528E) at room temperature for ca. 5 min. The capillary was flame sealed approximately 1 cm from the funnel end and hermetically sealed with 5-min epoxy (Harduran Inc.). To equilibrate the sample with added water, the sealed capillaries were placed in an oven at 95–100 °C for 30 min and cooled for 10 min at 21 °C. This heating/cooling cycle was repeated 5 times.

To monitor sample temperature during the real-time measurements, it was necessary to position a thermocouple (copper/constantan, Teflon covered, 0.003 in. in diameter, Omega) in the sample close to the bottom of the capillary. This was possible only for samples containing excess water where the thermocouple could be forced through the hydrated lipid. To this end, the sealed end of the capillary containing equilibrated lipid was removed, the thermocouple inserted into the lipid, and the capillary along with the thermocouple leads sealed with 5-min epoxy.

X-ray Diffraction. (*A*) *X-ray Source.* Most of the experiments to be described were carried out by using wiggler-enhanced, monochromatic (1.5 Å), focused X-rays on the A1 line at CHESS as previously described (Caffrey, 1984; Caffrey & Bilderback, 1984; Caffrey & Feigenson, 1984). A cylindrically bent single crystal of silicon (111) and a long float glass mirror was used for monochromatization and horizontal focusing, providing 2×10^9 photons/s down a 0.3-mm collimator (Supper) at 5.4 GeV and 22 mA of electron beam current. All measurements were made with CESR operating in the 3-bunch mode at 5.4 GeV and a total electron beam current of 20–35 mA.

In addition to using synchrotron radiation, some of the static measurements were made with nickel-filtered, unfocused Cu Kα (1.5428 Å) X-rays from a sealed tube anode (Model XRG-3000, Phillips Electronic Instruments) at 30 kV and 38 mA or from a rotating anode (Rigaku) at 40 kV and 8 mA.

Throughout these experiments, radiation damage to the samples was minimized by implementing the precautions outlined in an earlier publication (Caffrey, 1984).

(*B*) *Static X-ray Diffraction Measurements.* Diffraction patterns were recorded on X-ray-sensitive film (CEA Reflex 25, CEA America Corp.) using a Buerger Precession camera (Supper) with a 0.3-mm diameter collimator. Sample temperature was controlled to ±0.5 °C by placing the capillary in a brass holder through which water from a water bath was circulated. At the synchrotron source, exposure times varied from 2 to 8 min at a sample to film distance of 75 mm. With the sealed tube and the rotating anode, exposure times varied from 1 to 14 h at a sample to film distance of 50–75 mm.

(*C*) *Real-Time X-ray Diffraction Measurements.* The method used to record X-ray diffraction in live time along with the characteristics of the system has been described (Caffrey & Bilderback, 1983, 1984; Caffrey, 1984). Briefly, a Buerger Precession camera was used for the purpose of aligning the collimator, sample, and beam stop. The cassette holder and drive mechanism was removed to make way for a three-stage image intensifier tube (Varo), the real-time imaging device. The intensifier was operated at 5–7 V, and unless otherwise noted, measurements were made in the linear region of the detector (Caffrey & Bilderback, 1983). Dynamic display and recording of diffraction patterns were effected by using a vidicon comera (Sony AVC-1400 with a 25-mm Cosmicar TV lens, 1:1.9, no. 1929), monitor (Hitachi-Denchi), and cassette recorder (Panasonic, Omnivision II, Model NV-8310). Sample temperature, elapsed time in minutes, seconds, and number of frames were simultaneously recorded along with the X-ray diffraction pattern by using a character generator (Chronolog, serial no. S92,131-55-11234) interfaced to a digital voltmeter (thermometer) and electronic clock. To obtain quantitative recorded image intensity, an image processor (Grinnell image display buffer, Model GMR-274) was used as previously described (Caffrey & Bilderback, 1983). Unless otherwise noted, intensity information was obtained after averaging over three frames, equivalent to a 100-ms time slice. One-dimensional scans were made on samples displaying a true powder pattern such that orientation effects in the capillary were not important. Diffracted peak area, which should be proportional to the concentration of the phase under consideration, was determined by a triangular approximation as the product of peak height and full-width at half-maximum peak height. Only two phases coexisted at any one time, and throughout the transition, the sum of the normalized peak areas from the coexisting phases remained approximately constant. This result demonstrates the lack of orientation effects in all phases, the detector linearity, and the proportionality between diffracted peak area and phase concentration. Except for frame averaging, the raw, uncorrected data are presented.

Intrinsic rise and decay times for the real-time diffraction detection system were measured as previously described (Caffrey & Bilderback, 1983). While a lipid diffraction pattern in real time was recorded, the X-ray shutter in the monochromator cave was closed, and the signal intensity decay with time was measured by using the image processing technique. In a like manner, rise time was determined after the X-ray shutter was opened. The intrinsic rise and decay curves are included in Figure 6. Shutter opening and closing times are 1.8 and 1.7 ms, respectively, for the 0.3-mm collimator.

Prior to making the kinetic measurements, we determined the empirical phase diagram for the DHPE/water system using the real-time X-ray diffraction method. Sample capillaries were placed in a brass holder through which water from a temperature-regulated water bath could be circulated. A window of Kapton (0.0005 in., Du Pont) through which the incident and diffracted X-rays passed provided a sealed chamber for the same capillary. Attached to the brass holder was a 50-W resistance heater (Dale) whose output was regulated by a variable transformer. With the circulating water bath off, the resistance heater was turned on, and the sample temperature began to rise. Temperature was monitored by placing a thermocouple close to where the X-ray beam intercepted the same capillary. Simultaneously, X-ray dif-

fraction from the sample was recorded in real time. Lipid phase identification was based on both low- and wide-angle diffraction patterns, and changes in diffraction indicated crossing of a phase boundary. Occasionally, static diffraction measurements were made on film to confirm lipid phase identification. To cool the sample, the resistance heater was turned off, and the sample was allowed to cool slowly in air, or more rapidly by turning on the circulating water bath which had been set to ≤20 °C. Heating rates of 5–10 °C/min were used in these measurements.

Temperature Jump. A modification of the heat gun method used previously (Caffrey & Bilderback, 1983, 1984) and as implemented by Grubb et al. (1984) was employed to rapidly adjust the sample temperature from that of ambient to some predetermined value. Briefly, the temperature of the air stream from a heat gun was set by using a temperature controller (Eurotherm, type 812). The controller regulated heat gun heater output, and a feedback loop was provided by a thermocouple centered in the air stream leaving the heat gun barrel. The heat gun was allowed to reach set point with the air stream directed away from the sample. Temperature jump was effected by activating a solenoid which deflected the heat gun to a position where air flow was centered about, coaxial with and about 2 cm from the tip of the sample capillary. Air stream temperature was uniform over an area 1.3 × 1.3 cm at a distance of 1 cm from the center of the heat gun spout. Cooling occurred passively in air when a second solenoid was activated to deflect the heat gun away from the sample. Air flow was held constant, and so sample heating rate was altered only by changing the controller set point. Sample temperature was recorded as millivolts by using a thermocouple on a home-built, low-noise voltmeter with a sampling rate of 33 s^{-1}, i.e., at video frame rates, with a resolution of 0.01 mV (0.3 °C) in conjunction with a type T cold junction compensator (Omega).

Results

Empirical Phase Diagram Determination. Information on the general phase properties of the lipid as a function of water content and temperature was required before carrying out kinetic measurements on the DHPE/water system. Real-time X-ray diffraction is well suited for such measurements and was used in conjunction with static measurements to establish phase identity and boundaries. Phases and phase transitions were determined by recording low- and wide-angle X-ray diffraction in real-time as a function of temperature for samples prepared at a variety of hydration levels. The results are presented in Figure 1. The phase diagram is similar in its overall features to that reported for other ether PE derivatives as determined by calorimetry, X-ray diffraction, and ^{31}P NMR measurements (Seddon et al., 1983a, 1984). In excess of ca. 12% (w/w) water, three phases are seen in the temperature range 30–90 °C. At low temperatures, a lamellar gel phase ($L_{\beta'}$ or L_β) gives way to a lamellar liquid-crystalline phase (L_α). The stable form at higher temperatures is the hexagonal phase. Throughout this paper, use of the term hexagonal phase refers to the inverted hexagonal (H_{II}) phase as defined by Luzzati (1968). At saturating water levels, Seddon et al. (1984) report a lamellar chain-melting transition temperature of 68.5 °C and a lamellar/hexagonal transition temperature of 86 °C for DHPE which are close to the values obtained in the present study. Above 12% (w/w) water, a separate L_α phase is discernible over a finite temperature range. However, below this hydration level, the two adjacent transitions ($L_{\beta'}/L_\alpha$ and L_α/H_{II}) approach one another, and the L_α phase is no longer apparent. Thus, at low water levels, the conversion from

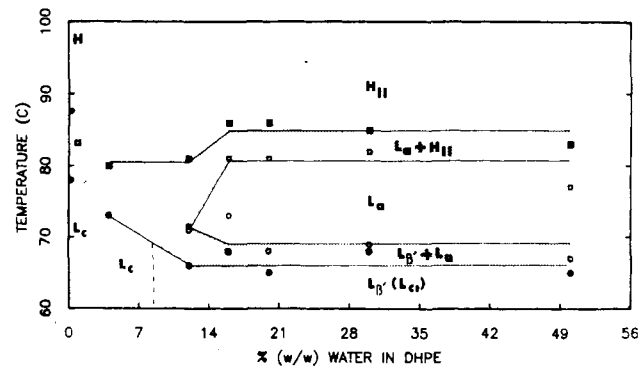

FIGURE 1: Phase properties of dihexadecylphosphatidylethanolamine/water as determined by a combination of static and live-time X-ray diffraction. Phase type and boundaries were identified upon sample heating at a rate of 5–10 °C/min. Methods used in sample preparation and data acquisition are described under Experimental Procedures. Identification of the H phase at high temperatures in the absence of added water is tentative, and the lattice type of the intervening fluid hydrocarbon phase is unknown. See text for details. Phase behavior between 0% and 4% water was not determined.

lamellar gel to hexagonal phase occurs without the intervention of the L_α phase as has been observed previously for some other lipid systems (Marsh & Seddon, 1982).

In general, the lamellar chain-melting transition temperature was found to decrease with increasing degree of hydration while that of L_α/H_{II} tended to increase with a leveling off from 16–20% (w/w) water (Figure 1). Phase coexistence was observed over finite temperature ranges at all phase boundaries. This is not an artifact of the relatively fast heating rates used in these measurements. For example, at 30% (w/w) water phase, coexistence at both transitions was monitored by the real-time method and was found to be stable for at least 2 min when sample temperature was held constant at a temperature intermediate between the two limiting or boundary values. Under these conditions, it was noted that the lamellar chain-melting transition was sharp with a width (ΔT) of approximately 1 °C. In contrast, the L_α/H_{II} transition was quite broad with a ΔT = 5–6 °C. The data shown in Figure 1 are for the heating curve. The phase boundaries identified upon relatively rapid cooling are shifted by 2–3 °C to lower temperatures. Interestingly, at and above ca. 30% (w/w) water, the (001) lattice spacing of the L_α phase is shorter than the $(10\bar{1}0)$ lattice spacing of the H_{II} phase, whereas below this level of hydration the opposite is true. Presumably, therefore, the $d_{(001)}$ and $d_{(10\bar{1}0)}$ spacings can be equalized by adjusting the water content.

These results demonstrate the usefulness of the real-time X-ray diffraction method in phase diagram construction. The data in Figure 1 were obtained in less than 2 h of continuous data collection.

To determine the nature of the acyl chain packing in the lamellar gel phase, some static X-ray diffraction measurements using X-ray-sensitive film were made on DHPE as a function of hydration level at 21 °C (Figure 2). The results are presented in Table I. The lamellar spacing (d) was found to increase up to 16% (w/w) water, and thereafter a constant d spacing of approximately 6.0 nm was obtained. Therefore, 16% (w/w) water is considered to be the limiting hydration level in agreement with the results of Seddon et al. (1984). These workers found limiting hydration of 16% and 17% water for the L_β and $L_{\beta'}$ phases of didodecyl-PE and diarachinoyl-PE, respectively. At hydration levels of 16% (w/w) water and above, the wide-angle region displayed a single symmetrical line at 0.405 nm (Figure 2B). At 0% and 8% (w/w) water, multiple wide-angle lines were observed, the strongest of which

Table I: Structural Parameters of the Lamellar Phases Adopted by Dihexadecylphosphatidylethanolamine/Water at 21 °C

degree of hydration [% (w/w) added water]	bilayer thickness (nm)	water layer thickness (nm)	acyl chain tilt angle (deg)	phase assignment[a]	wide-angle spacing[c] (nm)
0	5.44	0	ND[d]	L_C	0.46 M, 0.41 VS, 0.38 S
8	5.26	0.50	ND	L_C	0.46 VW, 0.41 VS, 0.38 S
16[b]	5.03	1.00	25	$L_{\beta'}$	0.41 VS
25	5.03	1.00	25	$L_{\beta'}$	0.41 VS
40	5.03	1.00	25	$L_{\beta'}$	0.41 VS

[a] Phases were assigned on the basis of the wide-angle X-ray diffraction pattern and on the calculated chain tilt angle in the case of $L_{\beta'}$. For L_C, the angle of tilt was not determined, and phase assignment was based on wide-angle diffraction alone (see text for details). [b] Above 16% (w/w) water, it is assumed that the chemical composition of the lipid phase remains constant and equal to that at the limiting hydration level of 16% (w/w) water. [c] Diffracted intensity is denoted as follows: VS, very strong; S, strong; M, medium; W, weak; VW, very weak (see Figure 2). [d] ND, not determined.

appeared at 0.41 and 0.38 nm, reminiscent of the "crystalline" (L_C) PE phase described by Seddon et al. (1983a, 1984). On the basis of the similarity, this phase is referred to as L_C in the present study. To determine the angle of tilt of the acyl chains at higher hydration levels, it was assumed that the d spacing observed at 16% (w/w) water corresponded to the limiting hydration level and that the addition of water beyond this level appears in the excess water phase. It is also assumed that the chains are not interdigitated. Following the procedure of Luzzati (1968) and Small (1967) [see also Seddon et al. (1984)], bilayer thickness (d_l), water layer thickness (d_w), average interfacial surface area per lipid molecule (S), and angle of tilt (θ) of the acyl chains were calculated. At 21 °C, the partial specific volume for water is 1.002 $mL \cdot g^{-1}$ (CRC Handbook, F-11), and for DHPE, a literature value of 0.96 $mL \cdot g^{-1}$ was used (Seddon et al., 1984). At limiting hydration, the calculated structural parameters were $d_l = 5.03$ nm, $d_w = 1.0$ nm, and $S = 0.417$ nm^2. The cross-sectional area per pair of acyl chains (S_c) can be calculated from the wide-angle spacing by assuming hexagonal chain packing which for $d = 0.405$ nm corresponds to $S_c = 0.189$ nm^2. The angle of tilt is then given by $\theta = \cos^{-1}(2S_c/S) = 25°$. This result shows that the acyl chains are tilted and that the lamellar gel phase is of the $L_{\beta'}$ rather than the L_β type. In like manner, Seddon et al. (1984) present evidence for tilted acyl chains in the case of hydrated diarachinoyl-PE in the lamellar gel phase. It should be mentioned that a single symmetrical wide-angle line is consistent with chain tilt provided the cross-section perpendicular to the acyl chains displays hexagonal symmetry (Tardieu et al., 1973; Mitsui, 1978).

These experiments were carried out by using the synchrotron source where X-ray exposure times are on the order of minutes. When similar measurements were made on DHPE at 60% (w/w) water using a rotating anode source where the exposure time was 12–15 h, the single, sharp line at $(0.41 \text{ nm})^{-1}$ was replaced by two sharp lines at $(0.47 \text{ nm})^{-1}$ and $(0.43 \text{ nm})^{-1}$. These two lines do not correspond to the wide-angle reflections observed in the L_C phase. However, they indicate a more orderly packing of the acyl chain than obtains in the $L_{\beta'}$ phase, and so this phase will be designated L_{C1} to distinguish it from the L_C phase seen at less than full hydration. It appears, therefore, that the $L_{\beta'}$ phase is metastable. A similar observation has been made for the L_β phase of didodecyl- and dilauroyl-PE (Seddon et al., 1983a,b, 1984). From a limited number of experiments carried out with DHPE at 60% (w/w) water, it appears that once the L_{C1} phase forms it is stable at temperatures up until chain melting occurs. However, upon cooling from L_α, the $L_{\beta'}$ phase forms and only with time below the chain-melting transition temperature does it revert to the L_{C1} phase. The long-term stability of L_{C1} was not examined.

Unless otherwise noted, the real-time X-ray diffraction experiments described below were carried out by starting with $L_{\beta'}$ as the low-temperature lamellar phase.

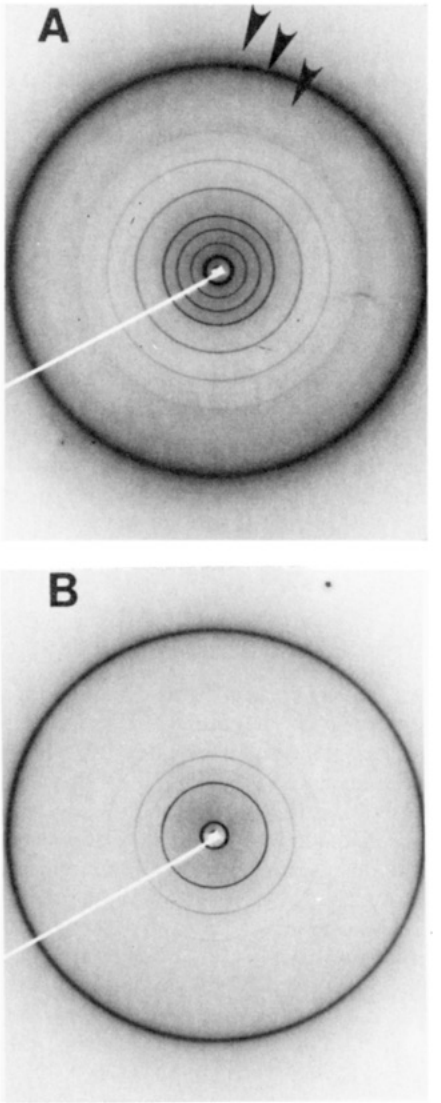

FIGURE 2: Diffraction pattern of dihexadecylphosphatidylethanolamine at 8% (A) and 16% (w/w) (B) water recorded on X-ray-sensitive film at 21 °C. In (A), the wide-angle lines at $(0.46 \text{ nm})^{-1}$, $(0.41 \text{ nm})^{-1}$, and $(0.38 \text{ nm})^{-1}$ are indicated by arrowheads. In (B), the single, wide-angle line is at $(0.405 \text{ nm})^{-1}$. Experimental conditions used in making these synchrotron radiation exposures include the following: sample to film distance, 75 mm; X-ray wavelength, 0.15 nm; collimator diameter, 0.3 mm; incident flux, 2×10^9 photons s^{-1}; electron beam current, 20 mA; machine energy, 5.4 GeV; exposure time, 3 min.

For anhydrous DHPE below 78 °C, a lamellar phase with multiple sharp lines in the wide-angle region, designated L_C after Seddon et al. (1984), is observed. Between 78 and 87 °C, chain melting occurs. The lattice type and symmetry of the newly formed phase designated α were not identified be-

cause of an inability to index the observed low-angle lines. Above 94 °C, another phase forms which displays two low-angle lines with spacings in the ratio $1:1/\sqrt{3}$. This is tentatively identified as a hexagonal phase and is designated H. Upon cooling from 100 °C to below 78 °C, the L_C phase forms almost immediately, i.e., with no evidence for an intermediate $L_{\beta'}$ or L_β phase. This observation is based upon real-time measurements in the wide-angle region.

Kinetic Measurements. The kinetic measurements described below are concerned primarily with the $L_{\beta'}/L_\alpha$ and L_α/H_{II} phase transitions in both the heating and cooling directions. Brief mention will be made of the direct $L_{\beta'}/H_{II}$ transition and of the phase changes undergone by "dry" DHPE. Most of the measurements were carried out with DHPE at 60% (w/w) water where the L_α phase is intermediate between the $L_{\beta'}$ and H_{II} phases. Furthermore, neither transition is purely isothermal, and phase coexistence was observed over a finite temperate range. Heating was active in the sense that heat was applied to the sample in order to raise sample temperature. On the other hand, cooling was passive and occurred in air upon removal of the heat source.

Sample temperature was simultaneously recorded during heating and cooling via a thermocouple positioned in the sample next to the X-ray beam. The fast response (170 °C·s^{-1}) of the thermocouple was evidence by the rapidity with which it responds to a large temperature jump when held in air (Figure 3). With the thermocouple in a capillary containing water alone, the exponential temperature rise was determined by the temperature and flow rate of the air stream, the diameter of the capillary, the proximity of the thermocouple to the leading edge of the capillary, and the thermal conductivity and apparent specific heat of the sample. When placed in the DHPE/water sample, there is a very obvious break in the heating curve at 67 °C, the main chain-melting temperature. At this temperature, heat input is being used to effect chain melting rather than to raise sample temperature. It is only after completion of chain melting that the sample temperature starts to rise again. The difference in the exponential slopes above and below the main chain-melting temperature (see inset of Figure 3I) probably reflects a somewhat greater specific heat in the $L_{\beta'}$ phase compared to the L_α phase [cf. Wilkinson & Nagle (1982) and Blume (1983)].

No evidence of the L_α/H_{II} phase transition was seen in the heating curve for DHPE/water probably because of the fast heating rates used, and because the transition is relatively broad (see above) and has an enthalpy change considerably (5×) less than that of the $L_{\beta'}/L_\alpha$ transition in excess water (Seddon et al., 1983a). Similar observations were made in the (passive) cooling curve; namely, the $L_{\beta'}/L_\alpha$ but not the L_α/H_{II} transition was seen as a break in the curve.

The real-time X-ray diffraction measurements made on a sample of DHPE at 60% (w/w) water are presented in Figures 4 and 5. Figure 4 shows the raw data, namely, low-angle diffraction recorded in live time as a function of time and temperature through the $L_{\beta'}/L_\alpha$ and L_α/H_{II} phase transitions following a temperature jump from ca. 30 to 93 °C. The reverse process, i.e., transition through H_{II}/L_α followed by the $L_\alpha/L_{\beta'}$ transition in the passive cooling mode, is also shown. The quantitative intensity information obtained by image processing is presented in Figure 5. In the low-temperature region at 37 °C, for example, the $L_{\beta'}$ phase alone is seen as a low-angle lamellar (001) reflection with a d spacing of 6.0 nm. Seddon et al. (1983a) report a value for fully hydrated DHPE of ca. 5.9 nm at 64 °C. Upon heating, the d spacing decreases in a continuous manner to a value of 5.8 nm at 66

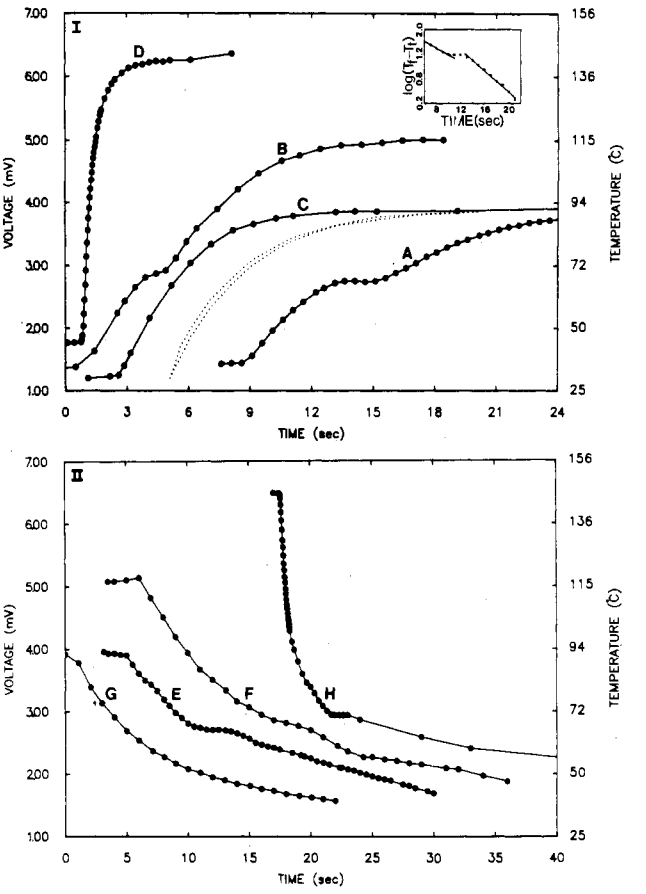

FIGURE 3: Sample temperature change with elapsed time after commencement of heating (I) and cooling (II). Heating was effected by rapidly deflecting the air stream from a heat gun onto the sample capillary, and cooling occurred passively in air when the air stream was deflected off the sample. Measurements were made with a thermocouple in capillaries containing DHPE/60% (w/w) water (A, B, E, and F), in water alone (C and G), or in air (D and H). The insert shows curve A plotted as log ($T_f - T_t$) vs. elapsed time where T_t and T_f correspond, respectively, to instantaneous and final sample temperature. The dotted curves in panel I were calculated on the basis of a 30–92 °C temperature jump in a 1-mm capillary containing DHPE/60% (w/w) water as described in the Appendix. The upper and lower curves correspond to calculated perimeter and center-line sample temperatures, respectively. Temperature jumps were to 92 °C (A, C, E, and G), 125 °C (B and F), and 155 °C (D and H). Curves are displaced along the abscissa for clarity.

°C. Continued heating effects phase transformation from $L_{\beta'}$ to L_α, and over a narrow temperature range, the long spacings from both phases coexist. With time and heating, the conversion proceeds with the intensity in the $L_{\beta'}$ line decreasing accompanied by a corresponding increase in the intensity of the L_α line. A graphical representation of these results is presented in Figure 6. At the chain-melting transition, the change in d spacing is discontinuous since the L_α lamellar repeat first appears at 5.1 nm while the last vestiges of the $L_{\beta'}$ phase have a d spacing of ~5.75 (Figure 7). The phase change seen by real-time X-ray diffraction occurs at the same temperature as the break seen in the heating curve described above (Figure 3). When chain melting is complete and as sample temperature continues to rise, the lamellar repeat for the L_α phase decreases continuously from 5.1 nm at 66 °C to 4.8 nm at 83 °C. At 76 °C, the first sign of the H_{II} phase is apparent. The intensity of the H_{II} $(10\bar{1}0)$ line grows at the expense of that in the L_α (001) line with continued heating until all of the intensity in the L_α line has disappeared. Like the $L_{\beta'}/L_\alpha$ transition, the L_α/H_{II} phase change is discontinuous. The $(10\bar{1}0)$ line of the H_{II} phase has a long spacing of 5.7 nm

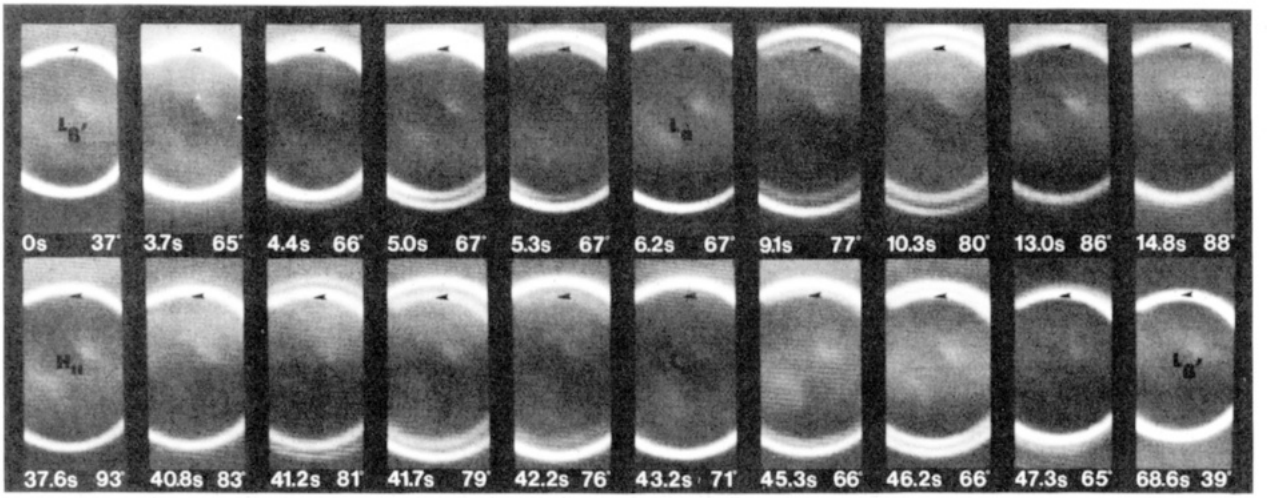

FIGURE 4: Dynamics of the lamellar gel/lamellar liquid-crystalline and lamellar liquid-crystalline/inverted hexagonal phase transformations in dihexadecylphosphatidylethanolamine at 60% (w/w) water following a temperature jump from 37 to 93 °C and subsequent passive cooling to 39 °C. Low-angle diffraction corresponding to the $L_{\beta'}$ (001), L_α (001), and H_{II} ($10\bar{1}0$) reflections was recorded by using the real-time X-ray diffraction method. Each photograph in the composite represents a single frame (33 ms) of the video-recorded images. Elapsed time and corresponding sample temperature (in degrees centigrade) after the commencement of heating are shown at the bottom of each frame. Passive cooling began at ca. 40 s. The arrowhead marks the position of the $L_{\beta'}$ (001) reflection at 37 °C before the temperature jump and is included as a reference point.

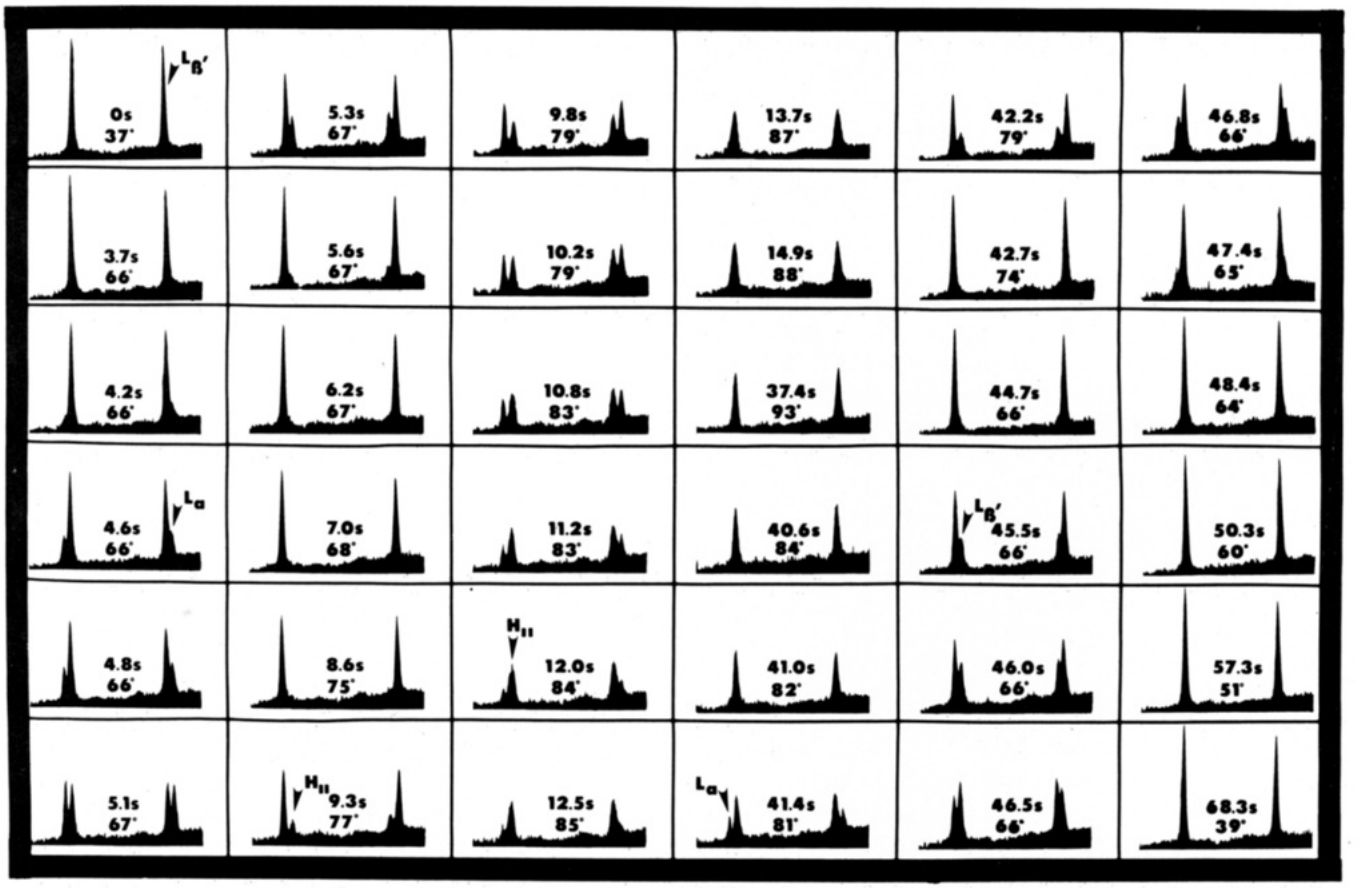

FIGURE 5: Kinetics of the lamellar gel/lamellar liquid-crystalline and lamellar liquid-crystalline/inverted hexagonal phase changes undergone by dihexadecylphosphatidylethanolamine at 60% (w/w) water following a temperature jump from 32 to 93 °C and subsequent changes upon passive cooling to 39 °C. Low-angle diffraction was recorded in real-time and computer processed to obtain diffracted intensity profiles as described under Experimental Procedures. Profiles were obtained from images representing the average of three video frames (equivalent to 100 ms at 30 frames·s^{-1}). Elapsed time and corresponding sample temperature are indicated.

at 77 °C and a negative temperature coefficient. By 93 °C, the long spacing has decreased to a value of 5.4 nm. The L_α/H_{II} transition is considerably less sharp than that of the $L_\alpha/L_{\beta'}$ transition as evidenced by phase coexistence over a larger temperature range.

Upon cooling, the reverse process occurs. The long spacing of the H_{II} phase increases continuously until the L_α/H_{II} phase transition temperature range is reached at which point a discontinuous change in *d* spacing is observed as the (001) line of the L_α phase appears and the H_{II} ($10\bar{1}0$) line fades. With time, the L_α phase alone is present, and its *d* spacing increases continuously until the main chain-melting transition temperature is reached. Here, the $L_{\beta'}$ phase forms at the expense of the L_α phase, and the *d* spacing of the low-temperature

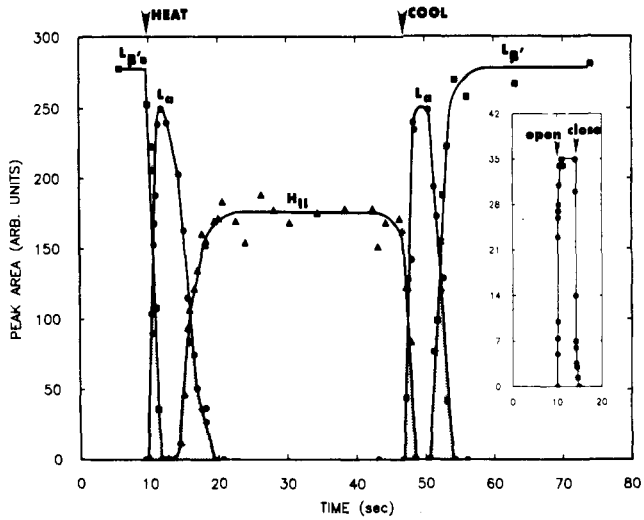

FIGURE 6: Kinetics of the phase changes undergone by dihexadecylphosphatidylethanolamine at 60% (w/w) water in response to a temperature jump from 30 to 93 °C. Low-angle X-ray diffraction was recorded in real-time and integrated intensity was obtained by image processing as described under Experimental Procedures. Each data point corresponds to an average over three consecutive frames (100 ms). The heating and cooling regime is indicated in the upper portion of the figure. Shaded areas represent regions of phase coexistence. The intrinsic rise and decay curves for the real-time imaging system are included on the right-hand side of this figure. Opening and closing of the X-ray shutter are indicated. See text for details.

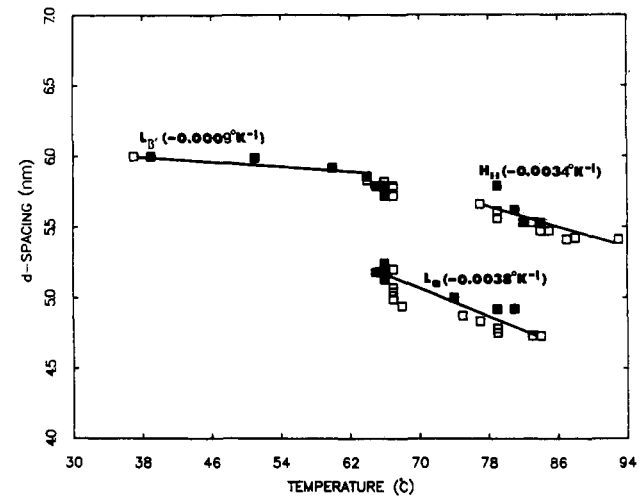

FIGURE 7: Lattice spacing of the lamellar gel ($L_{\beta'}$), lamellar liquid-crystalline (L_α), and inverted hexagonal (H_{II}) phases of dihexadecylphosphatidylethanolamine at 60% (w/w) water as a function of temperature during a temperature jump experiment from 30 to 93 °C. Solid symbols denote heating; open symbols denote cooling. The values in parentheses represent thermal lattice coefficients $[(1/d)\partial d/\partial T]$ calculated from the slopes of the lines at 50 °C ($L_{\beta'}$), 70 °C (L_α), and 86 °C (H_{II}).

phase increases continuously with cooling to the original value of 6.0 nm observed before the onset of heating. This process of heating and cooling was repeated many times and was found to be perfectly reproducible.

Real-time X-ray diffraction measurements were also made in the wide-angle region wherein changes in the short-range order at the acyl chain packing level can be followed (data not shown). The chain-melting transition occurred at 66 °C as was observed in the low-angle region and was evidenced by a change from a sharp, symmetrical line at 0.41 nm characteristic of the ordered gel phase to a diffuse line centered at ca. 0.46 nm reminiscent of a fluid hydrocarbon. Comparing the time dependence of the phase changes recorded at low and

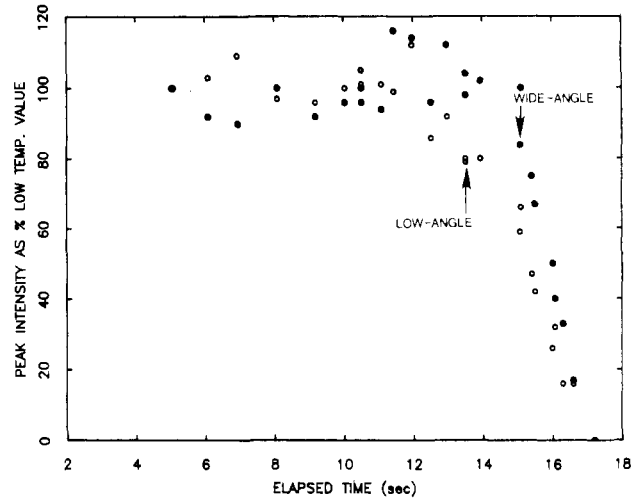

FIGURE 8: Kinetics of the change in long- (○) and short-range order (●) of the lamellar phase through the chain-melting transition of dihexadecylphosphatidylethanolamine in 60% (w/w) water during a temperature jump from 30 to 93 °C. Low- and wide-angle X-ray diffraction corresponding to the long- and short-range order was recorded simultaneously in real-time. Diffracted intensity information was obtained by image processing the recorded images. Each data point corresponds to an average over three consecutive frames (100 ms). Plotted intensity corresponds to peak height above background of the low-angle $L_{\beta'}$ (004) reflection and that of the wide-angle line at ca. (4.1 Å)$^{-1}$ as described in the text.

wide angles simultaneously shows that upon heating there is a loss in long-range order fractionally before chain melting occurs (Figure 8).

The data presented in Figures 4 and 5 document changes occurring in the low-angle region of the diffraction pattern for $2\theta \leq 2°$. Recordings were also made at shorter sample to detector distances such that the angular range examined extended out to $2\theta = 6°$ (Figure 9). With this arrangement, the (004) line of the lamellar phase and the $(11\bar{2}0)$ and $(20\bar{2}0)$ lines of the H_{II} phase could be seen quite clearly. However, these lines were not strong, and it is difficult to say with complete certainty what the temporality of the intensity changes in these lines was as related to those occurring in the (001) and $(10\bar{1}0)$ reflections. From a visual inspection of the recorded material, it did appear that the changes paralleled one another quite closely.

The experiment described above was carried out with a heat gun air temperature setting of 95 °C. Under these conditions, the $L_{\beta'}$ to L_α transition was complete in ≤2 s (Table II). Increasing the heat gun air temperature decreased the time required for the sample to undergo the chain-melting transition. At air temperature settings of 125 and 135 °C, the time required to undergo the transition, namely, the gross transit time (defined in footnote *c*, Table II), was reduced to ≤1 s. The reverse reaction upon cooling took place at a rate which was essentially independent of *final* heating temperature. Under all conditions, the L_α to $L_{\beta'}$ transition was complete within 6 s. It should be pointed out, however, that throughout these experiments the cooling process is a passive one.

The lamellar/hexagonal phase transition took place in a time interval which was dependent on the size of the temperature jump. The larger the jump, the shorter the time required to undergo the transition. At air temperature settings of 95 and 135 °C, the measured transit times were 5 and 1 s, respectively (Table II). Upon cooling, the hexagonal to lamellar transition occurred at ≤2 s at all temperatures except 95 °C where the transit time was 3 s. It is emphasized here that the measured transit times also include the time required to (1) heat/cool

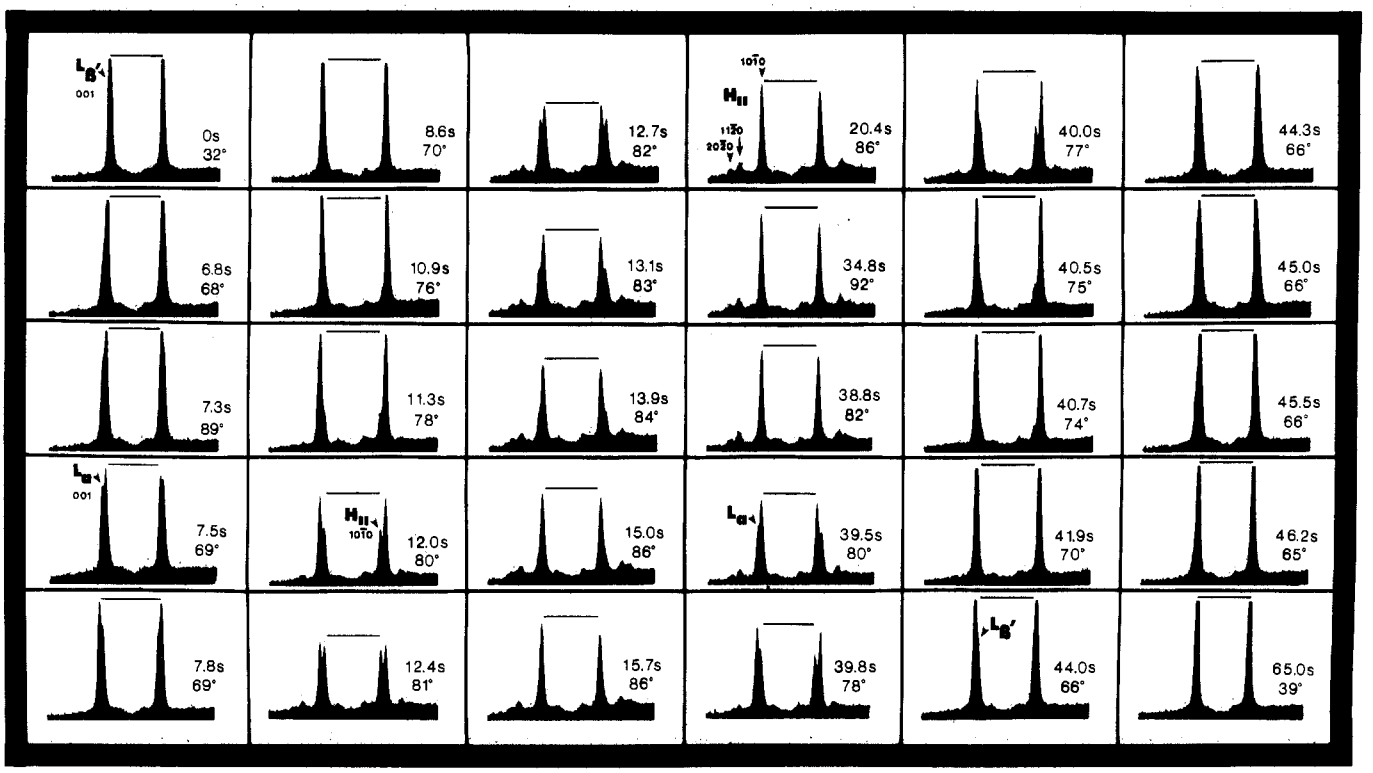

FIGURE 9: Kinetics of the lamellar gel/lamellar liquid-crystalline and lamellar liquid-crystalline/inverted hexagonal phase changes undergone by dihexadecylphosphatidylethanolamine at 60% (w/w) water following a temperature jump from 32 to 92 °C and subsequent changes upon passive cooling to 39 °C. Experimental conditions are as described in the legend to Figure 5 except that these measurements were made at a sample to detector distance of approximately 9 cm such that the $(11\bar{2}0)$ and $(20\bar{2}0)$ reflections of the inverted hexagonal phase could be seen simultaneously under these conditions. However, the detector saturated on the lamellar gel and liquid-crystalline (001) reflections, and resolution at low angles is poor. A bar corresponding to the diameter of the $L_{\beta'}$ (001) reflection at 32 °C is included above each profile for reference purposes.

Table II: Transit Time of the Various Thermotropic Phase Transitions Undergone by Hydrated and Nonhydrated Dihexadecylphosphatidylethanolamine in Response to a Temperature Jump[a]

degree of hydration [% (w/w) added water]	temperature jump[b] (°C)	diffraction angle	transit time[c] (s)					
			heat	heat	heat	cool	cool	cool
			$L_{\beta'} \rightarrow L_\alpha$		$L_\alpha \rightarrow H_{II}$	$H_{II} \rightarrow L_\alpha$		$L_\alpha \rightarrow L_{\beta'}$
60	95	low	2		5	3		3[g]
	125	low	1		2	1		3
	135	low	1		1	2		3
	95	wide	1					6[g]
25	95	low	2		5	1		3
16	95	low	2		4	1		2
12	125	low	2		1	2		3
				$L_C \rightarrow H_{II}$			$H_{II} \rightarrow L^d$	
8	95	low		5			4	
	135	low		2			5	
	155	low		1			5	
			$L_C \rightarrow \alpha$[e]		$\alpha \rightarrow H$[f]		$\alpha \rightarrow L_C$	
0	110	low	6					
	130	low	1		2			
	130	wide	2				4	

[a] Progress of the transition was monitored by low- and wide-angle real-time X-ray diffraction. [b] Temperature jump refers to the temperature of the heat gun air stream. Temperature jumps of 95, 105, 110, 115, 125, 135, and 155 °C resulted in final sample temperatures of 93, 99, 104, 111, 121, 126, and 146 °C, respectively. [c] Transit time refers to the time it takes to undergo the indicated phase change as judged by visual inspection of the video-recorded real-time X-ray diffraction images. Transit time is the time interval between the first sighting of diffraction from the newly forming phase and the last detectable diffraction from the phase undergoing the transformation. The transit times reported are gross values and include the time required to (1) heat/cool the sample through the transition temperature range, (2) supply/remove the latent heat of the transition, and (3) undergo the transition, i.e., the intrinsic or net transit time. Thus, the intrinsic transit time is always less than the measured gross value. [d] The identity of the lamellar phase (L_C, $L_{\beta'}$, or L_β) first formed upon cooling from the hexagonal phase was not determined. [e] The wide-angle data show this to be the chain-melting transition. The lattice type in the fluid phase (α) was not determined. [f] The phases involved in this transition are not known. The high-temperature phase is tentatively identified as hexagonal (see text for details). [g] The discrepancy between wide- and low-angle measurements arises because of the reduced sensitivity of the diffraction method to diffuse scatter as elaborated on in the text.

the sample through the transition temperature range and (2) supply/remove the latent heat of the transition. Thus, the intrinsic or net transit time of the phase transition is always less than the measured gross transit time.

At the lower heating rates, the mechanism of both the $L_{\beta'}/L_\alpha$ and L_α/H_{II} phase transitions in either the heating or

the cooling direction appears to be two state to within the sensitivity limits of the method. By two state, I mean that at any time during the transition no more than two phases coexist. At the chain-melting transition, diffraction lines from both phases on either side of the transition remain sharp through the transition, indicating that long-range order is maintained throughout the transition. No other low-angle scattering is observed other than that from the $L_{\beta'}$, L_α, and H_{II} phases either as additional sharp lines or as diffuse scatter. However, as with static X-ray diffraction measurements (Caffrey & Feigenson, 1984), the real-time method is also relatively insensitive to diffuse scatter, and small amounts would go undetected. The line widths of the lamellar reflections of the L_α and $L_{\beta'}$ phases did not undergo significant changes either before or during the transition. Thus, it appears as though both transitions are mechanistically quite simple: at any time during the transition, the coexisting phase types are either $L_{\beta'}$ and L_α or L_α and H_{II}. Intermediate states, if present, are at low occupancy and do not accumulate to detectable levels. This result is somewhat surprising in view of the dramatic topological changes undergone during these two transitions. In the lamellar transition, both the bilayer and water layer thickness can change, and the hydrophobic region of the bilayer undergoes tremendous alteration from ordered to highly disordered acyl chain packing. The changes accompanying the L_{α}/H_{II} phase transition are even more dramatic, involving gross structural rearrangements from a lamellar one-dimensional periodic phase to a hexagonal phase which is periodic in two dimensions.

A remarkable feature of these transitions is that the long-range order of the three lipid phases is preserved to a considerable extent. This is revealed by the observed maintenance of sharp diffraction lines throughout the transition. At 37 °C, the full width at half-maximum height (FWHM) of the $L_{\beta'}$ (001) reflection is 1.2 mrad (0.067°, $\Delta\theta/\theta = 0.09$), and that of the L_α (001) reflection is 1.3 mrad ($\sim$0.073°, $\Delta\theta/\theta = 0.08$) at 68 °C. Line width does not change appreciably through the $L_{\beta'}/L_\alpha$ transition, suggesting that long-range order in the newly forming phase is very rapidly established regardless of the direction through the chain-melting transition. Thus, large numbers of stacked lamellae presumably undergo the transition together in a highly cooperative manner which seems somewhat surprising in view of the considerable changes undergone during the transition at the level of acyl chain packing, surface area per molecule, and lipid bilayer and water layer thickness. The cooperativity of the chain-melting transition has been determined from calorimetry in a number of hydrated lipid species. However, since calorimetry is detecting ΔH_{cal} which primarily derives from changes in the short-range organization of the lipid acyl chains, it is less sensitive to changes in long-range order through the transition. As these real-time X-ray diffraction measurements show, under present conditions, such changes in long-range order through the transition, if they occur at all, are quite small. Following the analysis of Marsh et al. (1977), a cooperative unit size of 85 and a cooperativity index of 1.4×10^{-4} were obtained for the $L_{\beta'}/L_\alpha$ transition. The calculation is based on the assumption that the chain-melting transition broadening is strictly due to cooperative unit size effects and that the transition is a pseudounimolecular reaction with equilibrium constant $K = \gamma/1 - \gamma$ where γ corresponds to the degree of transition. γ is calculated as the peak intensity of the $L_{\beta'}$ (001) line divided by the sum of the peak intensities of the $L_{\beta'}$ and L_α (001) lines at various temperatures through the transition temperature range. In calculating the cooperative unit size, a literature value of 7.9 kcal·mol^{-1} was used for the ΔH_{cal} of fully hydrated DHPE (Seddon et al., 1983a). A physical interpretation of the cooperativity values calculated on the basis of the low-angle diffraction line intensity changes through the transition remains unclear. However, similar values have been obtained from calorimetry for other phospholipids dispersed in excess water (Marsh et al., 1977). The narrowness of the transition temperature range suggests that the process is a highly cooperative one. By the same token, the cooperativity of the L_α/H_{II} transition is considerably less than that of the $L_{\beta'}/L_\alpha$ transition, since the former occurs over a much wider temperature range.

The fact that the low-angle lamellar reflections remain sharp throughout the transition suggests that stacks of lamellae remain coupled and undergo the $L_{\beta'}/L_\alpha$ transformation together. This same maintenance of long-range order in the lamellar phase is seen for the L_α/H_{II} transition regardless of the direction in which the transition is approached. However, at the upper transition, the $(10\bar{1}0)$ line of the H_{II} phase first formed is considerably broadened, and only with time and continued heating does the line sharpen (Figures 4 and 5). At the beginning of the transition (ca. 77 °C), FWHM of the H_{II} $(10\bar{1}0)$ line is 2.0 mrad (0.12°, $\Delta\theta/\theta = 0.15$). After some time at 93 °C, the corresponding value is 1.4 mrad (0.08°, $\Delta\theta/\theta = 0.10$), indicating a considerable ordering of the hexagonal lattice. Upon cooling, the degree of order established at the higher temperature is maintained down to the L_α/H_{II} transition. For example, at 81 °C, FWHM of the $(10\bar{1}0)$ line is 1.5 mrad (0.09°) where significant levels of the L_α phase had already begun to accumulate. These comments refer to the situation at the lowest heating rates used. As the heating rate increased, so too did the degree of disorder prevailing in the first formed H_{II} phase. With time and continued heating, long-range order was restored to the hexagonal phase and, as for the lower heating rates, was preserved into the H_{II}/L_α transition upon cooling.

Thus far, I have described the kinetics and mechanism of the $L_{\beta'}/L_\alpha$ and L_α/H_{II} phase transitions occurring in DHPE at 60% (w/w) water. Measurements were also carried out at lower hydration levels and with unhydrated DHPE. The transit times through the various transitions as a function of hydration level and final sample temperature are included in Table II. Down to 12% (w/w) water, the transition kinetics and indeed the mechanism are similar to those observed at 60% (w/w) water. In brief, the shortest transit times recorded for the two transitions in either heating or cooling directions appear to be independent of hydration level from 12% to 60% (w/w) water.

At 8% (w/w) water, the lamellar/hexagonal transition is simultaneously accompanied by chain melting; i.e., there is no intermediate L_α phase (Figure 1). Thus, the phase transformation represents changes not only in lattice periodicity but also in short-range order at the acyl chain level. The transition was found to be as fast as either the $L_{\beta'}/L_\alpha$ or the L_α/H_{II} phase transitions observed in isolation at the higher hydration levels. At the 8% hydration level, real-time X-ray diffraction measurements in the wide-angle region were not carried out to confirm the identity of the low-temperature phase formed after the temperature jump experiment. It is assumed that the cooling transition is back to the L_C phase rather than to a metastable $L_{\beta'}$ phase, for example, as was observed with fully hydrated DHPE. Support for this comes from the observation that the d spacing of the first-order lamellar repeat was the same before and after the heat/cool cycle.

In the case of unhydrated DHPE, the chain-melting transition was identified by following changes in low- and wide-angle X-ray diffraction using the real-time method (Figure 1). The transition appears to take place over a relatively wide temperature range beginning at 78 °C and terminating at 88 °C. While the low-temperature lamellar phase is identified as being of the L_C type, i.e., with a crystalline acyl chain packing arrangement, the nature of the higher temperature phases has not been determined as described above. However, the transit times through these phase boundaries are included in Table II for completeness. Once again, the values are not noticeably different from those observed in the presence of added water.

Discussion

The two transitions examined in the present study are quite different in terms of the structural parameters that undergo change. The low-temperature transition at and above 12% (w/w) water involves chain melting in a lamellar phase. The high-temperature transition involves a large topological transformation from a one- to a two-dimensional lattice in the liquid-crystal state. This transformation can also involve simultaneous chain melting (see Figure 1 and Table II). The remarkable feature of these two transitions is the apparent ease with which both occur. In the case of fully hydrated DHPE, the chain-melting transition has an associated ΔH_{cal} = 7.9 kcal·mol^{-1} (Seddon et al., 1983a) and is therefore energetically expensive. However, it occurs quite fast and without any apparent loss in long-range order (see Figures 4 and 5). It is readily reversible and is quite repeatable. The same applies to the high-temperature L_α/H_{II} transition which is energetically less expensive (ΔH_{cal} = 1.5 kcal·mol^{-1}; Seddon et al., 1983a) but equally fast, reversible, and repeatable. Long-range order in the H_{II} phase is established somewhat more slowly than is observed with the $L_{\beta'}/L_\alpha$ transition. However, once it is established, it is maintained and lost only when the sample is cooled to below the lamellar/hexagonal transition temperature. The changes undergone in the lamellar gel/liquid-crystalline transition all occur within the lamellar phase. It does not seem unreasonable, therefore, that the transition occurs on a relatively short time scale, assuming there are no major alterations in water content of the two phases. In contrast, the high-temperature transition involves a change in periodicity from one to two dimensions. Thus, from a geometric point of view, the transition from the lamellar to the hexagonal phase seems much more complicated. In order for the process to occur with the ease with which it appears to take place, some simple topological connections between the two phases must obtain. This would obviate the need for large molecular rearrangements which might be energetically expensive or kinetically quite slow. In Figure 10 is presented a model for the DHPE lamellar/hexagonal phase transition which involves relatively small changes in positions of lipid and water molecules, does not require extensive exposure of hydrocarbon chains to the aqueous phase, sets up the hexagonal packing arrangement which is coplanar with the lamellar phase, and is directly reversible, and once inverted rod formation has been initiated in one direction, it can continue at an accelerating rate laterally from this direction throughout the sample volume. The model incorporates many of the experimental observations made on the L_α/H_{II} transition using the real-time X-ray diffraction method.

The lamellar phase is stabilized by molecules with a dynamically averaged cylindrical geometry while the inverted hexagonal phase prefers molecules that can fill a (truncated) wedge-shaped space which is the basic unit of volume that makes up a cylinder (Figure 11) (Israelachvili et al., 1976, 1977, 1980; Cullis & DeKruijff, 1979; Weislander et al., 1980;

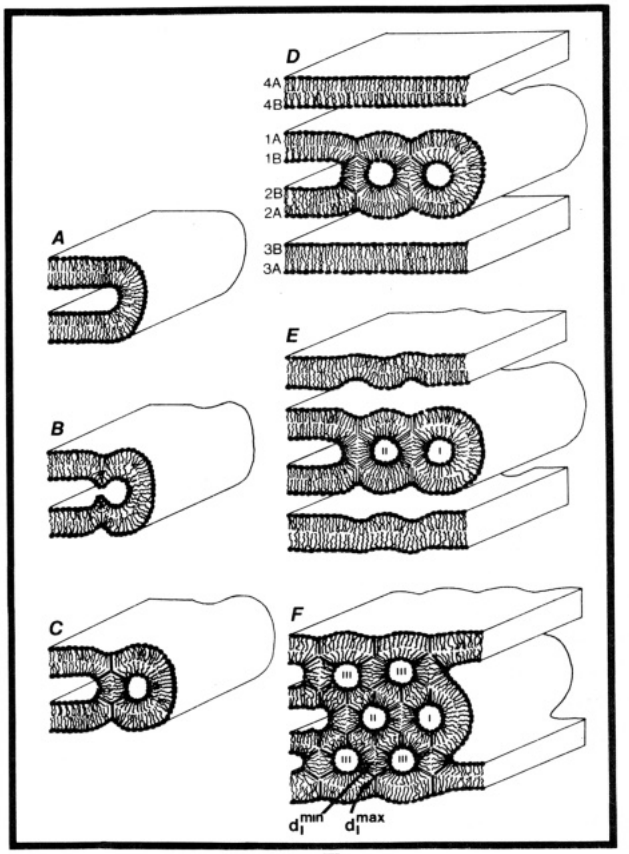

FIGURE 10: Schematic illustration of the proposed model for the lamellar/inverted hexagonal phase transition. Shown in (A) is a bilayer folded back on itself providing a region of high curvature and a site of H_{II} phase initiation. Adjacent bilayers have been omitted for clarity. Water occupies the space between bilayers and fills the central core of the inverted hexagonal phase cylinders. For simplicity, the dimensions of these two aqueous compartments have been set equal. Such a situation can arise in practice, and when it does, the lamellar to hexagonal transition is accompanied by net lipid dehydration. Regions where acyl chains experience maximum and minimum extensions are denoted d_l^{max} and d_l^{min}, respectively. Refer to the text for complete details.

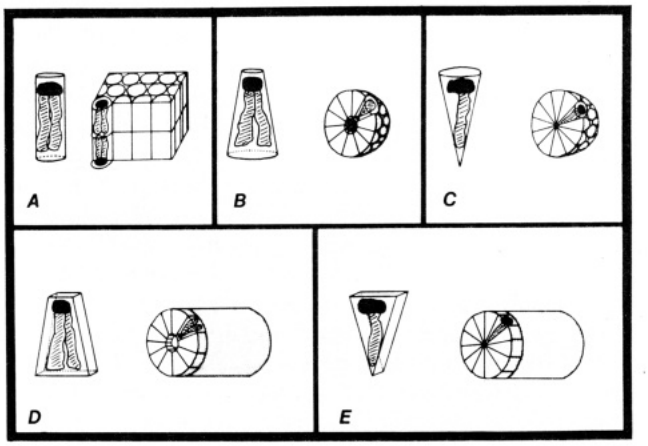

FIGURE 11: Schematic view of the dynamically averaged structure of lipids and their packing geometry. (A) Rod or cylindrically shaped molecules pack as extended bilayers; (B) truncated cone-shaped molecules packed as inverted micelles; (C) cone-shaped molecules pack as micelles; (D) truncated wedge-shaped molecules pack as extended hydrophobic cylinders as in the H_{II} phase; (E) wedge-shaped molecules pack as extended hydrophilic cylinders as in the H_I phase. Note: shape denotes the geometry of the volume available to the molecule in the lipid aggregate and does not imply a rigid molecular architecture.

Eibl, 1984). It is emphasized that use of the term shape does not imply a rigid structure of well-defined geometry but rather a dynamically averaged volume that constitutes the fundamental unit of the structure in question. As the lamellar/hexagonal transition temperature is approached from below, the wedge packing becomes energetically more favorable than the cylindrical packing. It is possible that hexagonal phase formation from the lamellar phase takes place at a point between two planar bilayers although it is probably more likely that it begins at a region of the bilayer which has folded back on itself. In this region, the inner leaflet of the bilayer is highly curved (see Figure 10). The high curvature lowers the free energy of the lipid since it accommodates the natural tendency of the molecule to fill a wedge-shaped volume in the hexagonal phase. In contrast, those molecules in the planar region of the membrane would be in a higher energy state above the transition temperature since the packing geometry here is optimally suited to rod-"shaped" molecules. Thus, there is a tendency for molecules in the planar region of the bilayer to adopt the wedge shape geometry, and this is facilitated by the heat input into the system at the transition temperature. This is indicated in Figure 10 by a local dimpling inward of the planar region of the membrane which accentuates and eventually pinches off an isolated cylinder of water. Pinching off continues along the length of the folded-back region of the bilayer to produce an elongated cylinder. After this first step, what has been generated is a long cylinder of water with a coating of lipid molecules oriented as in an inverted micelle with head groups in the water channel and acyl chains directed radially away from the long axis of the cylinder. An adjacent region of high curvature has also been produced which can continue to generate more "water in oil" rods (Figure 10). Note, however, that during the dimpling process which eventually leads to an isolated water cylinder, lipid has been pulled away from the bilayer interior which could potentially lead to void formation. Presumably, a large void in the hydrophobic region cannot be supported, and so the adjacent outer leaflet of the bilayer distorts to form an inward dimple. This has two implications. (1) The lipid has a natural inclination for dimpling since an area of high positive curvature accommodates molecules which at and above the transition temperature have a tendency to fill a wedge-shaped volume. This dimpled region in leaflet 1A (Figure 10) now becomes a site for pinching off an additional water cylinder, with the remainder of the lipid coating the cylinder coming from leaflet 4B in the neighboring bilayer. It is important to remember that at the transition temperature (approached from below) molecules in planar leaflet 4B are increasingly more stable in the wedge shape and so readily participate in propagation of the hexagonal phase because by coating the water cylinder they now occupy a region of high positive curvature. (2) In like manner, growth of the H_{II} phase continues below the original site (labeled I in Figure 10) of H_{II} formation, and so the phase grows through the lipid bulk away from the nucleation site. As can be seen in Figure 10, the process of cylinder formation triggered by adjacent cylinders leads to a close-packed assembly and naturally generates the hexagonal lattice. The model also generates a hexagonal phase which is coplanar with the lamellar phase (Figures 10 and 12). This coplanarity has been experimentally observed with oriented egg phosphatidylethanolamine samples (M. Caffrey and Y. Shimoyama, unpublished results) and by Grunner et al. (1982, 1985b) with oriented photoreceptor membranes.

The attractive features of this model are that the molecular rearrangements and conformational changes involved in going

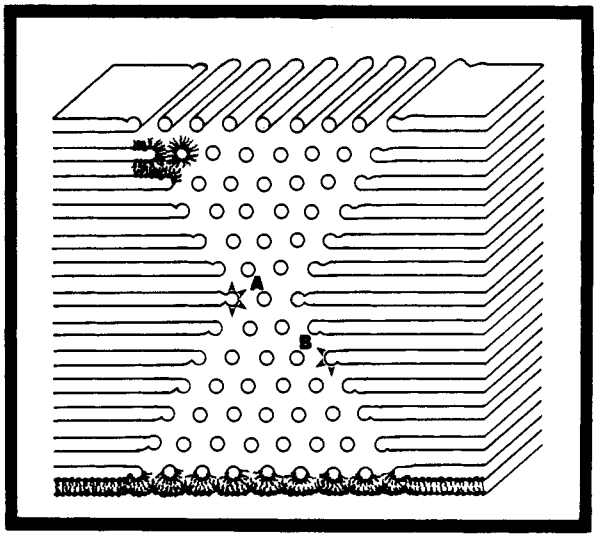

FIGURE 12: Schematic view of bulk inverted hexagonal phase growth from the lamellar phase. The first cylinder to form is shown at (A). It triggers the formation of four adjacent cylinders which in turn trigger the formation of six adjacent cylinders and so on throughout the bulk of the lipid. The lipid arrangement, shown at the bottom and at the top left-hand corner, is omitted in the rest of the diagram for clarity. The arrowheads at (A) and (B) correspond to directions of maximum acyl chain extension arising from adjacent hexagonal cylinders (d_l^{max} in Figure 10). Because of the greater number of adjacent cylinders, nascent cylinder formation will proceed faster at (A) than at (B). In this figure, the coplanarity of the coexisting phases is very obvious.

from one phase to the other are quite small. In addition, very little new hydrocarbon/water interface is created during the transition. Propagation can be fast and is cooperative in nature since each new cylinder generates new rod initiation sites (Figure 12). The process is readily reversible, requiring no new mechanism. Lowering the temperature would simply shift the free energy of the lipid molecule such that it packs more as a rod than a wedge in the lipid aggregate. The consequence of this shift would be to destabilize the region of high curvature in favor of planar packing. This has the effect of pulling lipid away from the hydrophobic core at the lattice point complementary to the water cylinders. As was noted for H_{II} phase formation, to prevent voids in the hydrophobic region, lipid molecules upon switching from wedge to rod shape reorganize to fill the potential void. In so doing, the isolated water cylinders fuse along their length to form a continuous, planar sheet of water separating continuous, planar lipid bilayers of the lamellar phase (Figure 10). This results in restoration of the original condition prevailing at low temperatures, including the orientation of the lamellae which started out (see Figure 10) parallel to the horizontal plane. It is possible, however, that growth of lamellae might continue at 60°, 120°, 180°, 240°, or 300° to this direction and so produce lamellae that are stacked at 60° or 120° with respect to the horizontal. This raises an interesting point because some of the samples examined in the present study were found to be partially oriented with the lamellar planes parallel to the long axis of the capillary in the $L_{\beta'}$ and L_α phases but apparently much less well oriented in the hexagonal phase. Upon cooling from the hexagonal phase, the original lamellar orientation was restored. From a fully oriented lamellar sample, one expects two sets of (001) reflections perpendicular to the plane of the lamellae. A correspondingly oriented hexagonal phase will yield six first-order reflections [(1,0), (0,1), (1,1), ($\bar{1}$,0), (0,$\bar{1}$), and (1,$\bar{1}$)] at 60° to one another with the (1,0) and ($\bar{1}$,0) reflections on the same axis as the (001) lamellar reflections. While two strong (001) reflections were seen in the case of the partially

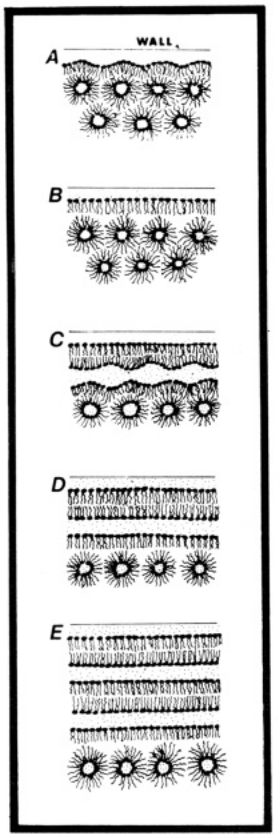

FIGURE 13: Schematic view of the lamellar/inverted hexagonal phase transition which restores the lamellar phase to its original low-temperature orientation parallel to the container wall. In (A), the lipid is in the hexagonal phase. Cooling proceeds from the wall inward, effecting the hexagonal → lamellar phase transition (B → E). the voids depicted in the hydrocarbon regions should be considered transient if they occur at all. It may be that the acyl chains extend to fill the voids and thus help propagate the transition as described in the text.

oriented $L_{\beta'}$ phase, in the H_{II} phase the diffraction pattern consisted of rings rather than six discrete spots and was more reminiscent of a pattern from a powdered hexagonal crystal. It may well be, however, that the hexagonal phase was somewhat orientationally disordered because it originated from an $L_{\beta'}$ phase which was not fully oriented to begin with. Thus, the H_{II} reflections were arched and as a result of overlapping took on the appearance of a powder pattern. The interesting point is that upon cooling from the hexagonal phase the original orientation of the $L_{\beta'}$ and L_{α} phases was restored rather than being displaced by 60° or 120° as might be expected from the above hexagonal model consisting of rods which are identical and crystallographically equivalent. This apparent memory of an earlier phase orientation may arise as a result of a nascent low-temperature phase which propagates radially inward to the center of the sample (Figure 13). This seems logical since in our present experimental arrangement the outer extremities of the sample will be the first to cool (Appendix). Thus, surface effects may dictate the initial direction of growth of the lamellar phase which then propagates inward parallel to the capillary walls in such a manner as to regenerate the original orientation of the low-temperature lamellar phase.

As noted earlier, the initial site of H_{II} cylinder formation is likely to be one of high curvature. However, cylinder formation might also take place between two opposed planar bilayers. For this to occur requires that the bilayer locally dimples. To evaluate the likelihood of this happening, an estimate of the energy cost of the dimpling process is needed. This can be done by assuming (1) that the dimple has the shape of a semicylinder of infinite length and has an inner radius of 2.18 nm as was determined for the H_{II} phase of fully hydrated DHPE (Seddon et al., 1984) and (2) that the lipid molecule is square in cross-section with a surface area (S) of 0.49 nm^2 (Seddon et al., 1984). The dimpling process is modeled as an elastic deformation of the membrane, assuming the bilayer to be incompressible (volume modulus of compressibility = 10^{10}–10^{11} dyn·cm^{-2}; Evans & Hochmuth, 1978). The work done in deforming the bilayer derives primarily from creating a hydrocarbon/water interface and in lowering the entropy of the lipid. The volume deformed for one lipid length h (where $h = \sqrt{S}$) of cylinder = $^1/_2\pi r^2 h$ = 5.2 nm^3, involving 9.5 phospholipid molecules or 0.55 nm^3 per molecule. Assuming an elastic thickness modulus of compressibility of 10^8 dyn·cm^{-2} (Evans & Hockmuth, 1978) or 2.4×10^{-21} cal·nm^{-3} implies an energy of deformation equal to 1.3×10^{-21} cal per molecule. This corresponds to approximately 1.1 kT per molecule at the L_{α}/H_{II} transition temperature and demonstrates that even for a flat bilayer such a deformation is possible. The case is much more favorable with DHPE at the high-temperature transition since the lipid molecules at this temperature are well suited to packing in a dimpled region of positive curvature. Those molecules at the base of the dimple and those meeting it at an angle of 120° from nearby cylinders are probably close to fully extended [see also Kirk et al. (1984) and Gruner et al. (1985b)]. This is energetically costly because of the limited number of conformations available in this state (Gruen, 1982; Hladky & Gruen, 1984). Also in that region of the upper leaflet linking the dimple to the planar portion of the same leaflet there is a region of negative curvature which is not well suited to accommodating H_{II}-tending molecules. In this region, however, the lipids are more likely to be rod shaped, and only when enough energy is pumped into the system through sample heating do they adopt the wedge shape and in so doing help to drive or propel the advancing front of H_{II} cylinder formation.

The propagation rate of the advancing H_{II} phase along any interlamellar water layer will depend on the phase type it is next to. For example, an isolated cylinder will grow more slowly than one surrounded on all sides by H_{II} phase cylinders due to the ability of adjacent cylinders to induce in nearby nascent cylinders regions of high positive curvature (Figures 10 and 12). The greater the number of nearest-neighbor cylinders, the faster the rate of nascent cylinder growth. For this reason, therefore, it is expected that the nascent cylinder next to A in Figure 12 will grow faster than that next to B. Gruner et al. (1985b) reach a similar conclusion in their treatment of lamellar/hexagonal phase coexistence in photoreceptor membranes.

Concerning the point raised earlier about acyl chain extension at complementary lattice sites of water cylinders in the H_{II} phase, I wish to make the following comments. Calculations based on the structural parameters for fully hydrated didodecylphosphatidylethanolamine (DDPE; Seddon et al., 1984) show that the length of the lipid molecule at the region of maximum extension (d_l^{max}) is 1.42 nm compared to a minimum extension (d_l^{min}) of 1.02 nm at a temperature of 135 °C (see Figure 10 for a description of d_l^{max} and d_l^{min}). The bilayer half-thickness in the L_{α} phase at 90 °C is 1.43 nm, and extrapolating to 135 °C (thermal lattice coefficient = −0.0018 K^{-1}; Seddon et al., 1984), a value of 1.30 nm is obtained. This, coupled with the fact that acyl chain conformation is considerably more disordered in the H_{II} phase compared to the L_{α} phase (Gally et al., 1980; Hardman, 1982; Casal & Mantsch, 1984), would serve to decrease d_l in the

H_{II} phase still further. Thus, the calculated d_l^{max} of 1.42 nm is certainly more extended than d_l predicted for the H_{II} phase. If, as a result of overextension, lipids in lattice sites complementary to the water cylinders are in a high-energy state, one might expect nonuniform diffusion rates around the circumference of the cylinders or differential partitioning of lipid species around the cylinder for a H_{II} phase prepared, for example, from two lipids differing in fatty acyl chain length. ^{31}P NMR spectra of the H_{II} phase have been interpreted as arising from motional averaging as a result of rapid lipid diffusion around the cylinder perimeters. However, there still remains some confusion as to the exact origin of such signals since the "characteristic" H_{II} ^{31}P NMR spectrum can be explained by the presence in a lamellar sample of (1) small amounts of cubic phase and (2) micelles and small unilamellar vesicles and by lamellar phase lipid in which there is a slight tilting of the head group away from the bilayer plane (Hui et al., 1980; Thayer & Kohler, 1981). It is important to note that the above arguments are based on the assumption that in the H_{II} phase the lipid head groups are rigidly fixed at the surface of the water cylinder which is assumed to be perfectly circular in cross-section and that fluctuations in lipid position perpendicular to the lipid/water interface are not allowed. Small fluctuations of this type presumably do occur (Hladky & Gruen, 1982, 1984). If so, this would then reduce the extent of acyl chain stretching at the complementary lattice sites and thus lower the free energy of the lipid molecules at these sites.

A mechanism for the lamellar/inverted hexagonal phase transition has recently been discussed in terms of an inverted micellar intermediate (Siegel, 1984). The model depicts inverted spherical micelles forming between two apposed membranes where each micelle is surrounded by a "semitorroidal" leaflet at its equator and by the outer leaflets of the originally apposed bilayers at the poles [Figures 2a and 3 in Siegel (1984)]. H_{II} phase formation was proposed to involve production of large numbers of these inverted micelles which diffuse laterally in the plane of the apposed bilayers, resulting in aggregation of micelles into strings and eventual fusion into H_{II} rods or cylinders. I argue against this mechanism on the following grounds.

(1) Diffusion of inverted micelles in the plane of apposed bilayers will be extremely limited because each inverted micelle is trapped or enveloped by the semitorroidal surface of the apposed bilayers. Thus, aggregation into a string of micelles which precedes fusion into H_{II} rods would require the cooperative motion of an enormous number of lipid molecules not only in the inverted micelle but also in the semitorroidal surfaces. Furthermore, before direct micelle/micelle contact can be made, the intervening semitorroidal surfaces must be ruptured. The probability of spontaneous side by side inverted micelle formation without an intervening surface is expected to be low.

(2) If the mechanism of the transition were to proceed via the inverted micellar intermediate followed by micellar aggregation, then growth of the H_{II} rods might be expected to be uncorrelated and to result in an assemblage of rods randomly distributed in the plane of the apposed bilayers. Thus, H_{II} phase formation would require that these random rods align with their long axis parallel. Of course, each micelle-derived H_{II} rod is isolated from its neighbor by an extended semitorroidal surface as was observed above for the isolated inverted micelles. Thus, close packing of rods would require rupture of these surfaces and consequently slow down the phase transformation process. If these postulated intermediates accumulate to a significant level, the transition would be accompanied by large amounts of diffuse scatter as detected by the real-time X-ray diffraction method. The experimental observations are that the transition is fast and two state to within the sensitivity limits of the real-time X-ray diffraction method, both of which argue against this mechanism for the DHPE system.

Estimates of the actual rates involved in these various processes have not been made. However, from the topological arguments presented above, it seems that bulk H_{II} phase formation from the lamellar phase might be an extremely cumbersome and therefore slow process if inverted micelles of the type described by Siegel (1984) are compulsory intermediates. The real-time X-ray diffraction measurements show this transition in DHPE to be fast and readily reversible. Thus, the mechanism proposed on the basis of these real-time observations seems more reasonable since the hexagonal lattice is directly generated and grows reversibly and cooperatively in all directions from the original initiation site(s). It is important to mention, however, that the rate of a phase transition probably reflects more the ease with which nucleation and water equilibration between the different phases occur than the complexity of the molecular rearrangements undergone during the transition. Siegel has recently proposed a variation of the inverted micellar intermediate coalescence model which seems more reasonable and is consistent with the observed L_α/H_{II} transit times (Siegel, 1985).

The proposed transition mechanism does not invoke intermediates such as inverted micelles. It is possible, however, that fixing the DHPE system during the transition may reveal the presence of inverted micellelike intermediates of varying lengths depending on the degree of rod elongation acquired at the moment of fixing. This model closely resembles the mechanism proposed by Hui et al. (1983) for the lamellar/hexagonal transition in PE/PC mixtures observed by freeze–fracture electron microscopy and ^{31}P NMR. In this study, one of the transitions was continuous from lamellar to hexagonal with insignificant quantities of intermediates accumulating during the conversion. Indeed, the electron micrographs reveal structures such as ripples continuous with smooth bilayers that are expected on the basis of the model depicted in Figures 10 and 12. Some of the other systems examined by Hui et al. (1983) accumulated intermediates during the transition. It should prove very instructive to make real-time X-ray diffraction measurements on these systems to determine if the method can detect such intermediates.

Many of the present temperature jump measurements were made with an air stream temperature of 95 °C which was sufficient to effect the L_α/H_{II} phase transition in all but the "dry" DHPE sample and was not too hot to significantly alter the water vapor pressure and thus the transition temperature inside the sealed capillary. Indeed, from the average pressure dependence of the L_α/H_{II} phase transition temperature observed for fully hydrated egg PE of approximately 0.05 °C·bar^{-1} (Chang & Yager, 1983; Yager & Chang, 1983), it can be shown that at the highest temperature used in the present study (155 °C), where the vapor pressure of water is 5.5 bar (CRC Handbook, D-169), the transition temperature would have increased by less than 1 °C.

To increase the rate of sample heating beyond that available with a preset temperature of 95 °C, the heat gun air temperature was raised (Figure 3). This had the effect of shortening the transit time through the two transitions (Table II). However, since the final sample temperature in each case was different, it could not be determined whether the reduced transit time reflects a response to the heating rate or to the

higher final sample temperature. The final temperature can affect the transit time by changing nucleation site formation and growth rate, water viscosity, lipid permeability, etc. This issue will have to be resolved in a separate study where the final sample temperature is held constant and the heating rate is varied.

Phase coexistence was observed at the chain-melting and at the lamellar/hexagonal transition of DHPE at 60% water in both heating and cooling directions. At no time, however, were there ever more than two phases coexisting even at the highest (preset temperature = 155 °C) heating/cooling rates examined. In this sense, the system is well behaved, and there is no violation of the phase rule. However, it is not necessary that the phase rule applies, since these are not necessarily equilibrium measurements. The phase rule forbids coexistence of three lipid phases ($L_{\beta'}$, L_α, H_{II}) and an excess water phase at any one temperature and pressure in a two-component system at equilibrium. However, at 12% (w/w) water where the two transitions are in close proximity (Figure 1) and where the heating rate was high (preset temperature = 125 °C), transient coexistence of three phases was seen. A small, short-lived temperature gradient through the sample along the direction of the X-ray beam would also account for this observation (see Appendix and Figures 14 and 15).

In an earlier communication, I described the kinetics and mechanism of the gel to liquid-crystalline phase transformation in DPPC at limiting hydration levels. The transition was apparently two state with a transit time of ≤2 s. The transition was not isothermal, and $L_{\beta'}/L_\alpha$ phase coexistence was observed over a finite temperature range. Similar observations were made in the present study of DHPE both above and below the $L_{\beta'}$ phase limiting hydration level of 16% (w/w) water. At the highest heating rate used in this study, the $L_{\beta'} \rightarrow L_\alpha$ transition occurred in 1 s and rose to 2 s at the lowest heating rate (Table II). Thus, while the maximum rate at which the transition can occur has not yet been determined, the results indicate that the $L_{\beta'} \rightarrow L_\alpha$ transition can occur at or under 1 s regardless of (1) lipid identity, (2) whether the acyl chain/glycerol linkage is of the ester or ether type, and (3) the degree of hydration (in the case of DHPE). Similar types of diffraction measurements have been carried out by Ranck and co-workers (Ranck et al., 1984) on microbial membranes and on membrane lipid extracts. Unfortunately, in-sample temperature was not monitored simultaneously with the diffraction measurements. Thus, the measured transition "delays" or "relaxation times" reported by Ranck et al. include not only the intrinsic transit time but also the time required to (1) heat or cool the sample through the transition temperature range and (2) supply or remove the latent heat of the transition. As is shown below, depending on the sample and the experimental arrangement, this can amount to a nontrivial time interval. Regardless of these difficulties, the results of the present study and those of Ranck et al. (1984) are in general agreement with regard to the kinetics of the lamellar/hexagonal transition.

In the present study, the cooling process was a passive one and occurred in air when the hot air stream was deflected away from the sample. Thus, the rate of sample cooling should be determined principally by the difference in sample and ambient air temperature. Since all of the upper sample temperatures used were ≤95 °C and since both transitions are below this temperature, a sample cooling rate below 95 °C is expected to be independent of the final sample temperature. Thus, if there is no effect of the latter on the mechanism of the cooling transitions, the recorded transit times should be independent of the final sample temperature for a given treatment. To within the sensitivity limits of the method, this appears to be the case (Table II).

In terms of transit times as used to characterize the various lipid transitions in Table II, the corresponding intrinsic decay and rise time values of the real-time apparatus are 0.8 and 0.5 s, respectively. Transit times on the order of 1 s were observed in the present study (Table II), indicating that the measurements are close to being detector limited. The fastest heating rate used in the present study was that attainable by using a heat gun air temperature of 155 °C. Generally, it was found that transit times decreased at higher sample heating rates and final sample temperatures, both of which changed together as described above. Since a limiting transit time was not observed, it is concluded that the values reported in Table II are upper limit values and that faster sample heating (and cooling) along with faster detection devices will be needed to determine the true limiting rates for these various transitions.

One concern in carrying out these temperature jump experiments is that the rate through the transition may be limited by heat transfer from the air stream to and through the sample. The empirical observation that transit times decrease with increasing heating rate (Table II) as effected by raising air stream temperature suggests that under present conditions heat transfer is limiting. However, it is important to reemphasize that the changing transit times may be a reflection of the final sample temperature as well as of the sample heating rate. The calculations that follow show that heat transfer may indeed be rate limiting. Contributing factors include the time it takes to (1) heat the sample through the transition temperature range and (2) supply the latent heat of the transition. An estimate of these two times can be made by assuming the heat transfer coefficient of the air stream is 37 $cal \cdot m^{-2} \cdot s^{-1} \cdot K^{-1}$, the sample diameter is 1 mm, the sample density is 10^6 $g \cdot cm^{-3}$, and the $L_{\beta'}/L_\alpha$ transition is at 66 °C and has a ΔH_{cal} = 7.9 $kcal \cdot mol^{-1}$ (see Appendix). For a DHPE sample at 60% (w/w) water, the time required to supply the latent heat at an air stream temperature of 92 °C is 1.3 s. The corresponding times at 125 and 155 °C are 0.6 and 0.4 s, respectively. At the L_α/H_{II} transition which has a transition temperature of approximately 83 °C and a ΔH_{cal} = 1.90 $kcal \cdot mol^{-1}$, the calculated times required to supply the latent heat of the transition are 0.8, 0.2, and 0.1 s at 92, 125, and 155 °C, respectively. The time required to heat the sample from 66 to 67 °C, i.e., through the $L_{\beta'}/L_\alpha$ transition, was calculated to be 0.4 s for an air stream temperature of 92 °C (Appendix). Therefore, at this relatively slow heating rate, it takes a total of 1.7 s, i.e., 1.3 + 0.4 s, to heat the sample through the transition and to transfer the latent heat of the transition to the sample. The experimentally determined transit time at this heating rate was 2 s. The agreement between the two values along with the observation that transit times decreased with increasing heating rate suggests that the limiting factor is heat transfer and not the lipid phase transition itself. This applies to the L_α/H_{II} phase transition also. For both transitions, the shortest recorded transit time is 1 s, suggesting that *the two lipid phase transitions can occur at ≤1 s*. It is obvious, therefore, that in order to identify the true limiting phase transit times faster sample heating rates are required.

Besides the intrinsic physicochemical interest in making measurements of lipid phase transition kinetics, there are some practical reasons for pursuing the present type of investigation. The real-time X-ray diffraction method can provide a limiting rate for a given transition. This, coupled with model studies of the type carried out by Siegel (1984, 1985), can be used to evaluate various proposed mechanisms for cellular processes

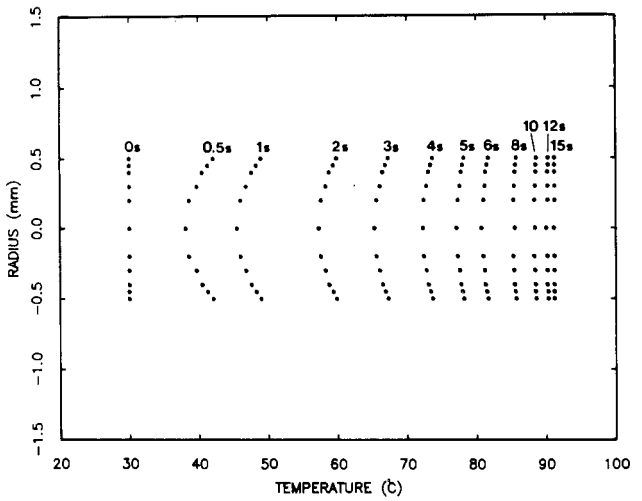

FIGURE 14: Calculated temperature profile across a 1-mm diameter capillary containing DHPE/60% (w/w) water as a function of time following a temperature jump from 30 to 92 °C. Details of the calculations are presented in the Appendix.

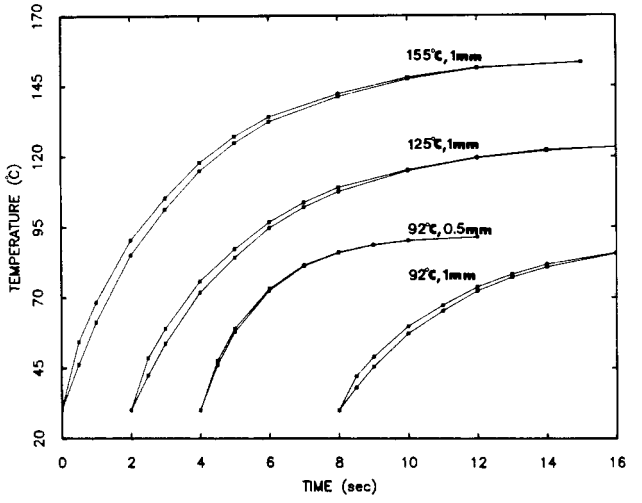

FIGURE 15: Calculated temperature change with time in a DHPE/60% (w/w) water sample as a function of the temperature jump size and capillary diameter. The upper and lower curves in a given pair correspond to the perimeter and center-line sample temperatures, respectively. Details of the calculations are presented in the Appendix. Curves are displaced along the abscissa for clarity.

such as membrane fusion. Mechanisms may refer to those occurring in pure lipid systems or by extension to certain physiological phenomena. The real-time method also allows us to examine the nature of the transition, whether it is a two- or a multi-state process. If it is of the latter type, then information on the number, identity, order of appearance, formation rates, half-lives, and occupancy of the intermediates can be obtained in addition to identifying the rate-limiting step. Limiting transit times should also prove useful in calculating effective freezing rates needed to "trap" different lipid phases during cryofixation procedures used in freeze–fracture electron microscopy, cryopreservation, and lyophilization. Diffraction is one of the few methods to provide information on long-range order within a sample. Thus, the degree to which long-range order and short-range order remain coupled through the various transitions can be determined by the real-time X-ray diffraction technique. If the transition mechanism can be established through the real-time method, repeating the measurement in the presence of a perturbant might reveal the manner in which the perturbing agent elicits its effect. Thus, real-time X-ray diffraction is a method with the potential for providing unique, time-resolved, structural information on changes undergone in response to a perturbation from one equilibrium state to another.

ACKNOWLEDGMENTS

I thank B. W. Batterman (National Science Foundation Grant DMR81-12822), D. H. Bilderback, G. W. Feigenson (National Institutes of Health Grant HL-18255), D. Har, C. Prior, and the entire CHESS staff for their invaluable help and support. Further thanks go to Ellen Patterson for carefully typing the manuscript, to J. K. Moffat for use of the sealed-tube and rotating anode X-ray sources (National Institutes of Health Grants GM29044 and RR-01646), to W. W. Webb for making available the Grinnell image processing system, to J.-H. Liu and D. T. Grubb for assistance with the temperature jump experiments, and to G. W. Feigenson, K. Florine, S. M. Gruner, Z. R. Korszun, V. A. Parsegian, D. P. Siegel, K. E. Torrance, and M. D. Yeager for critically reading the manuscript.

APPENDIX

To calculate the temperature profile along the sample capillary diameter as a function of time following a temperature jump, the following assumptions and approximations are made. (1) The sample consists of an infinite cylinder of diameter $d = 10^{-3}$ m prepared from DHPE at 60% (w/w) water. (2) Contributions from the 10^{-5}-m-thick glass walls of the capillary are negligible. (3) The sample is heated in cross-flow. (4) Air flow from the heat gun is turbulent. (5) Sample thermal diffusivity (α) is calculated at 75 °C and is used as though a temperature-independent term. The calculation is for an air flow rate (U_∞) of 2 m·s^{-1} and a temperature jump from 30 to 125 °C, i.e., initial sample temperature (T_i) = 30 °C and heat gun air temperature (T_∞) = 125 °C. The heat capacity (C_p) of DPPC and the thermal conductivity (k) of palmitic acid are used in these calculations since the corresponding values for DHPE are (to the author's knowledge) not available in the literature. Average sample thermal conductivity is calculated at 75 °C, midway through the temperature jump.

Connective Heat Transfer Coefficient of the Air Stream. To determine whether air flow around the capillary is laminar or turbulent, the Reynolds number (Re) must be calculated. $Re = \rho U_\infty d/\mu$. For air at 125 °C, we find that $\rho = 0.8826$ kg·m^{-3} and $\mu = 2.286 \times 10^{-5}$ kg·m^{-1}·s^{-1} (Holman, 1976). Thus, Re = 77, implying laminar flow. The average heat transfer coefficient (h) of air at 125 °C across the capillary can now be calculated as

$$h = \frac{kC\mathrm{Pr}^{1/3}}{d}\left[\frac{U_\infty d}{\nu}\right]^n$$

For air at 125 °C, $k = 0.03365$ W·m^{-1}·K^{-1}, Pr = 0.689, and $\nu = 25.9 \times 10^{-6}$ m^2·s^{-1} (Holamn, 1976). Since $40 \leq Re \leq 4000$, $C = 0.683$ and $n = 0.466$. Thus, $h = 154$ W·m^{-2}·K^{-1} at 125 °C. Additional calculations show that h varies from 153 to 157 W·m^{-2}·K^{-1} for temperatures of 77 and 153 °C, respectively. Thus, h is not strongly temperature dependent in this temperature range.

Average Thermal Conductivity of the Sample. The thermal conductivity of water (k_{water}) at 77 °C = 0.668 W·m^{-1}·K^{-1} (CRC Handbook, E-10). Since the thermal conductivity of DHPE (k_{DHPE}) is not available in the literature, the value for palmitic acid at 73 °C of 0.1714 W·m^{-1}·K^{-1} (4.097×10^{-4} cal·cm·cm^{-2}·s^{-1}·K^{-1}; CRC Handbook, E-4) will be used. For a sample consisting of 60% (w/w) water, the average thermal conductivity is

$$k = 0.4(0.1714) + 0.6(0.668) = 0.469\ \mathrm{W \cdot m^{-1} \cdot K^{-1}}$$

Axis Temperature as a Function of Time. The temperature $T(0,\tau)$ at the center line ($r = 0$) of the capillary at a given time (τ) can be calculated by using the Heisler chart (Holman, 1976). To use the chart it is necessary to calculate (A) $k/hr_0 = 6.1$ given the above values for k and h and the radius of the capillary $r_0 = 5 \times 10^{-4}$ m and (B) $\alpha\tau/r_0^2$ where τ is the elapsed time and α is the thermal diffusivity of the sample. $\alpha = k/\rho C_p$ where $k = 0.469\ \mathrm{W \cdot m^{-1} \cdot K^{-1}} = 0.469\ \mathrm{J \cdot m^{-1} \cdot s^{-1} \cdot K^{-1}}$; $\rho = 1\ \mathrm{g \cdot cm^{-3}} = 10^6\ \mathrm{g \cdot m^{-3}}$ and $C_p = 0.6C_p(\text{water}) + 0.4C_p(\text{DHPE})$. C_p(water) at 77 °C = 4.371 $\mathrm{J \cdot g^{-1} \cdot K^{-1}}$ (Holman, 1976) and C_p(DHPE) = C_p(DPPC) = 0.5 $\mathrm{cal \cdot g^{-1} \cdot K^{-1}} = 2.0925\ \mathrm{J \cdot g^{-1} \cdot K^{-1}}$ (Wilkinson & Nagle, 1982; Blume, 1983). Therefore, $\alpha = 2.24 \times 10^{-7}\ \mathrm{m^2 \cdot s^{-1}}$, and for $\tau = 1$ s, we get $\alpha\tau/r_0^2 = 0.9$. The Heisler chart for $\alpha\tau/r_0^2 = 0.9$ and $k/hr_0 = 6.1$ gives

$$\frac{\theta_0}{\theta_i} = \frac{T(0,\tau) - T_\infty}{T_i - T_\infty} = 0.75$$

and

$$T(0,\tau) = T(0,1) = 125 - 95(0.75) = 53.8\ ^\circ\mathrm{C}$$

Thus, 1 s after a temperature jump from 30 to 125 °C, the center-line temperature of the sample has reached 53.8 °C.

Off-Axis Temperature as a Function of Time. To calculate sample temperature at radial position r and time τ, the quantity θ/θ_0 must be obtained graphically for specified values of r/r_0 and k/hr_0. For example, if $r = 0.3$ mm, $r/r_0 = 0.6$ and $k/hr_0 = 6.1$, then $\theta/\theta_0 = 0.97$. Thus, $T(r,\tau) = T_\infty + (T_i - T_\infty)(\theta_0/\theta_i)(\theta/\theta_0)$ and $T(0.3,1) = 125 + (30 - 125)(0.75)(0.97) = 55.9$ °C. In this way, the temperature profile through the sample can be calculated at any time following a temperature jump. The results of one such calculation for a 30 to 92 °C jump are presented in Figure 14. In addition, the calculated sample temperature changes with time at the axis and at the perimeter of the capillary following temperature jumps from 30 to 92, 125, and 155 °C are presented in Figure 15. Also included in this figure is a comparison of the heating curves as a function of capillary diameter. Such plots allow us to calculate the time interval ($\Delta\tau$) between which a perimeter temperature of 66 °C and an axis temperature of 67 °C are attained for a given temperature jump. For example, for a jump to 92 °C:

$$\Delta\tau = \tau(0,67) - \tau(0.5,66) = 0.43\ \mathrm{s}$$

For DHPE at 60% (w/w) water, the $L_{\beta'}$ to L_α transition occurs at 66 °C and has a width of approximately 1 °C. From the above calculations, we would expect the transition to occur with a transit time in excess of 0.43 s since 0.43 s alone is required to heat the entire sample volume from 66 to 67 °C. In addition, the latent heat of transition must be supplied to the sample which will increase the transit time to >0.43 s. With a temperature jump to 155 °C, the corresponding $\Delta\tau$ value is 0.33 s. Thus, while the average sample heating rate increases by 3.4-fold in going from a 92 to 155 °C jump, the $\Delta\tau$ value is reduced by only a factor of 1.3. This probably reflects the higher temperature gradient in the sample at the 155 °C jump and the finite thermal conductivity of the sample.

Registry No. DHPE, 54285-60-8.

REFERENCES

Akiyama, M. (1981) *Biochim. Biophys. Acta 644*, 89–95.

Akiyama, M., Terayama, Y., & Matsushima, N. (1982) *Biochim. Biophys. Acta 687*, 337–339.

Albert, A. D., Sen, A., & Yeagle, P. L. (1984) *Biochim. Biophys. Acta 771*, 28–34.

Blume, A. (1983) *Biochemistry 22*, 5436–5442.

Boni, L. T., & Hui, S. W. (1983) *Biochim. Biophys. Acta 731*, 177–185.

Caffrey, M. (1984) *Nucl. Instrum. Methods Phys. Res. 222*, 329–338.

Caffrey, M., & Feigenson, G. W. (1981) *Biochemistry 20*, 1949–1961.

Caffrey, M., & Bilderback, D. H. (1983) *Nucl. Instrum. Methods Phys. Res. 208*, 495–510.

Caffrey, M., & Bilderback, D. H. (1984) *Biophys. J. 45*, 627–631.

Caffrey, M., & Feigenson, G. W. (1984) *Biochemistry 23*, 323–331.

Cameron, D. G., & Mantsch, H. H. (1982) *Biophys. J. 38*, 175–184.

Casal, H. L., & Mantsch, H. H. (1984) *Biochim. Biophys. Acta 779*, 381–401.

Chang, E. L., & Yager, P. (1983) *Mol. Cryst. Liq. Cryst. 98*, 125–129.

Chen, S. C., Sturtevant, J. M., & Gaffney, B. J. (1980) *Proc. Natl. Acad. Sci. U.S.A. 77*, 5060–5063.

Cho, K. C., Choy, C. L., & Young, K. (1981) *Biochim. Biophys. Acta 663*, 14–21.

Clegg, R. M., & Elson, E. L. (1975) *Biopolymers 14*, 883–887.

Corless, J. M., & Costello, M. J. (1981) *Exp. Eye Res. 32*, 217–228.

Crowe, L. M., & Crowe, J. H. (1982) *Arch. Biochem. Biophys. 217*, 582–587.

Cullis, P. R., & DeKruijff, B. (1979) *Biochim. Biophys. Acta 559*, 399–420.

Cullis, P. R., DeKruijff, B., Hope, M. J., Nayar, R., & Schmid, S. L. (1980) *Can. J. Biochem. 58*, 1091–1100.

Cullis, P. R., DeKruijff, B., Hope, J. M., Verkleij, A. J., Nayar, R., Tilcock, C. P. S., Madden, T. D., & Bally, M. B. (1983) in *Membrane Fluidity in Biology* (Aloia, R. C., Ed.) Vol. 1, pp 39–81, Academic Press, New York.

Dafler, J. R. (1977) *J. Am. Oil Chem. Soc. 54*, 249–254.

Das, S., & Rand, R. P. (1984) *Biochem. Biophys. Res. Commun. 124*, 491–496.

Dea, P., Pearson, L. T., Caffrey, M., Feigenson, G. W., & Chan, S. I. (1985) *Biochim. Biophys. Acta* (submitted for publication).

Deamer, D. W., Leonard, R., Tardieu, A., & Branton, D. (1970) *Biochim. Biophys. Acta 219*, 47–60.

DeKruijff, B., Verkleij, A. J., Lennissen-Bijvelt, J., Van Echteld, C. J. A., Hille, J., & Rijnbout, H. (1982) *Biochim. Biophys. Acta 693*, 1–12.

Dupont, Y., Gabriel, A., Chabre, M., Gulik-Krzywicki, T., & Schechter, E. (1972) *Nature (London) 238*, 331–333.

Eck, V., & Holzwarth, J. F. (1984) in *Surfactants in Solution* (Mittal, K. L., & Lindman, B., Eds.) Vol. 3, pp 2059–2079, Plenum Press, New York.

Eggers, F., & Funck, T. (1976) *Naturwissenschaften 63*, 280–285.

Eibl, H. (1984) *Angew. Chem., Int. Ed. Engl. 23*, 257–271.

Elamrani, K., & Blume, A. (1983) *Biochemistry 22*, 3305–3311.

Elamrani, K., & Blume, A. (1984) *Biochim. Biophys. Acta 769*, 578–584.

Evans, E. A., & Hochmuth, R. M. (1978) *Curr. Top. Membr. Transp. 10*, 1–64.

Fahey, P. F., & Webb, W. W. (1978) *Biochemistry 17*, 3046–3053.

Gally, H. U., Pluschke, S., Overath, P., & Selig, J. (1980) *Biochemistry 19*, 1638–1643.

Gordon-Kamm, W. J., & Steponkus, P. L. (1984) *Proc. Natl. Acad. Sci. U.S.A. 81*, 6373–6377.
Gounaris, K., Brain, A. P. R., Quinn, P. J., & Williams, W. P. (1983) *FEBS Lett. 153*, 47–52.
Grubb, D. T., Liu, J.-H., Caffrey, M., & Bilderback, D. H. (1984) *J. Polym. Sci., Polym. Phys. Ed. 22*, 367–378.
Gruen, D. W. R. (1982) *Chem. Phys. Lipids 30*, 105–120.
Gruenewald, B., Blume, A., & Watanabe, F. (1980) *Biochim. Biophys. Acta 597*, 41–52.
Gruenewald, B., Frisch, W., & Holzwarth, J. F. (1981) *Biochim. Biophys. Acta 641*, 311–319.
Gruner, S. M. (1985) *Proc. Natl. Acad. Sci. U.S.A. 82*, 3665–3669.
Gruner, S. M., Rothschild, K. J., & Clark, W. A. (1982) *Biophys. J. 39*, 241–251.
Gruner, S. M., Cullis, P. R., Hope, M. J., & Tilcock, G. P. S. (1985a) *Annu. Rev. Biophys. Biophys. Chem. 14*, 211–238.
Gruner, S. M., Rothchild, K. J., DeGrip, W. J., & Clark, N. A. (1985b) *J. Phys. (Les Ulis, Fr.) 46*, 761–769.
Gulik-Krzywicki, T., Aggerbeck, L. P., & Larsson, K. (1984) in *Surfactants in Solution* (Mittal, K. L., & Lindman, B., Eds.) Vol. 1, pp 237–257, Plenum Press, New York.
Hammes, G. G., & Tallman, D. E. (1970) *J. Am. Chem. Soc. 92*, 6042–6046.
Hardman, P. D. (1982) *Eur. J. Biochem. 124*, 95–101.
Harlos, K., & Eibl, H. (1980) *Biochim. Biophys. Acta 601*, 113–122.
Harlos, K., & Eibl, H. (1981) *Biochemistry 20*, 2888–2892.
Hladky, S. B., & Gruen, D. W. R. (1982) *Biophys. J. 38*, 251–258.
Hladky, S. B., & Gruen, D. W. R. (1984) *Biophys. J. 45*, 645–646.
Holman, J. P. (1976) *Heat Transfer*, 4th ed., McGraw-Hill, New York.
Holzwarth, J. F., Frisch, W., & Gruenewald, B. (1982) in *Microemulsions* (Robb, L. D., Ed.) pp 185–205, Plenum Press, New York.
Hui, S. W., Stewart, T. P., & Yeagle, P. L. (1980) *Biochim. Biophys. Acta 601*, 271–281.
Hui, S. W., Stewart, T. P., & Boni, L. T. (1981a) *Science (Washington, D.C.) 212*, 921–922.
Hui, S. W., Stewart, T. P., Yeagle, P. Pl., & Albert, A. D. (1981b) *Arch. Biochem. Biophys. 207*, 227–240.
Hui, S. W., Stewart, T. P., & Boni, L. T. (1983) *Chem. Phys. Lipids 33*, 113–126.
Inoue, S., Nishimura, M., & Yasunaga, T. (1981) *J. Phys. Chem. 85*, 1401–1405.
Israelachvili, J. N., Mitchell, D. J., & Ninham, B. W. (1976) *J. Chem. Soc., Faraday Trans. 2 72*, 1525–1568.
Israelachvili, J. N., Mitchell, D. J., & Ninham, B. W. (1977) *Biochim. Biophys. Acta 470*, 185–201.
Israelachvili, J. N., Marcelja, S., & Horn, R. G. (1980) *Q. Rev. Biophys. 13*, 121–200.
Jensen, J. W., & Schutzbach, J. S. (1984) *Biochemistry 23*, 1115–1119.
Johnson, M. L., Winter, T. C., & Biltonen, R. L. (1983) *Anal. Biochem. 128*, 1–6.
Kachar, B., & Reese, T. S. (1982) *Nature (London) 296*, 464–466.
Kirk, G. L., Gruner, S. M., & Stein, D. L. (1984) *Biochemistry 23*, 1093–1102.
Larsson, K., & Puang-Ngern, S. (1979) in *Advances in Biochemistry and Physiology of Plant Lipids* (Appelquist, L. A., & Liljenberg, C., Eds.) pp 27–33, Elsevier, New York.
Larsson, K., Fontell, K., & Krog, N. (1980) *Chem. Phys. Lipids 27*, 321–328.
Lentz, B. R., Freire, E., & Biltonen, R. L. (1978) *Biochemistry 17*, 4475–4480.
Luzzati, V. (1968) in *Biological Membranes, Physical Fact and Function* (Chapman, D., Ed.) Vol. 1, pp 71–123, Academic Press, New York.
Marsh, D. (1980) *Biochemistry 19*, 1632–1637.
Marsh, D., & Seddon, J. M. (1982) *Biochim. Biophys. Acta 690*, 117–123.
Marsh, D., Watts, A., & Knowles, P. F. (1977) *Biochim. Biophys. Acta 465*, 500–514.
Meyer, H. W. (1983) *Naturwissenschaften 70*, 251–252.
Miner, V. W., & Prestegard, S. H. (1984) *Biochim. Biophys. Acta 774*, 227–236.
Mitaku, S., Ikegami, A., & Sakanishi, A. (1978) *Biophys. Chem. 8*, 295–304.
Mitaku, S., Juppo, T., & Kataoka, R. (1983) *Biophys. J. 42*, 137–144.
Mitsui, T. (1978) *Adv. Biophys. 10*, 97–135.
Mollevanger, L. C. P. J., & DeGrip, W. J. (1984) *FEBS Lett. 169*, 256–260.
Nagle, J. F., & Wilkinson, D. A. (1982) *Biochemistry 21*, 3817–3821.
Navarro, J., Toivio-Kinnucan, M., & Racker, E. (1984) *Biochemistry 23*, 130–135.
Noordam, P. C., Van Echteld, C. J. A., DeKruijff, B., & DeGier, J. (1981) *Biochim. Biophys. Acta 646*, 483–487.
Owen, J. D., Hemmes, P., & Eyring, E. M. (1970) *Biochim. Biophys. Acta 219*, 276–282.
Persson, P. K. T. (1984) *Chem. Phys. Lipids 35*, 11–19.
Platt-Aloia, K. A., Bliss, R. D., & Thompson, W. W. (1983) in *Biosynthesis and Function of Plant Lipids* (Thompson, W. W., Mudd, J. B., & Gibbs, M., Eds.) pp 160–172, Waverly Press, Baltimore, MD.
Ranck, J. L. (1983) *Chem. Phys. Lipids 32*, 251–270.
Ranck, J. L., Mateu, L., Sadler, D. M., Tardieu, A., Gulik-Krzywicki, T., & Luzzati, V. (1974) *J. Mol. Biol. 85*, 249–277.
Ranck, J. L., Lattelier, L., Shechter, E., Krop, B., Pernot, P., & Tardieu, A. (1984) *Biochemistry 23*, 4955–4961.
Rand, R. P., & Sengupta, S. (1972) *Biochim. Biophys. Acta 255*, 484–492.
Ruocco, M. J., & Shipley, G. G. (1982a) *Biochim. Biophys. Acta 684*, 59–66.
Ruocco, M. J., & Shipley, G. G. (1982b) *Biochim. Biophys. Acta 691*, 309–320.
Sano, T., Tanaka, J., Yasumaga, T., & Toyoshima, Y. (1982) *J. Phys. Chem. 86*, 3013–3016.
Seddon, J. M., Cevc, G., & Marsh, D. (1983a) *Biochemistry 22*, 1280–1289.
Seddon, J. M., Harlos, K., & Marsh, D. (1983b) *J. Biol. Chem. 258*, 3850–3854.
Seddon, J. M., Cevc, G., Kaye, R. D., & Marsh, D. (1984) *Biochemistry 23*, 2634–2644.
Shipley, G. G. (1973) in *Biological Membranes* (Chapman, D., & Wallach, D. F. H., Eds.) Vol. 2, pp 1–89, Academic Press, New York.
Shipley, G., Green, J. P., & Nichols, B. W. (1973) *Biochim. Biophys. Acta 311*, 531–544.
Siegel, D. P. (1984) *Biophys. J. 45*, 399–420.
Siegel, D. P. (1985) *Biophys. J.* (in press).
Small, D. M. (1967) *J. Lipid Res. 8*, 551–557.

Sprague, S. G., & Staehelin, A. (1983) in *Biosynthesis and Function of Plant Lipids* (Thompson, W. W., Mudd, J. B., & Gibbs, M., Eds.) pp 144-159, Waverly Press, Baltimore, MD.
Strehlow, U., & Jahnig, F. (1981) *Biochim. Biophys. Acta 641*, 301-310.
Tardieu, A., Luzzati, V., & Reman, F. C. (1973) *J. Mol. Biol. 75*, 711-733.
Thayer, A. M., & Kohler, S. J. (1981) *Biochemistry 20*, 6831-6834.
Tilcock, C. P. S., Bally, M. B., Farren, S. B., Cullis, P. R., & Gruner, S. M. (1984) *Biochemistry 23*, 2696-2703.
Tsong, T.-Y. (1974) *Proc. Natl. Acad. Sci. U.S.A. 71*, 2684-2688.
Tsong, T.-Y., & Kanehisa, M. I. (1977) *Biochemistry 16*, 2674-2680.
Van Echteld, C. J. A., Van Stigt, R., DeKruijff, B., Leunissen-Bijvelt, J., Verkleij, A. J., & De Gier, J. (1981) *Biochim. Biophys. Acta 648*, 287-291.
Van Echteld, C. J. A., DeKruijff, B., Verkleij, A. J., Leunissen-Bijvelt, J., & De Gier, J. (1982) *Biochim. Biophys. Acta 692*, 126-138.
Van Venetie, R., & Verkleij, A. J. (1981) *Biochim. Biophys. Acta 645*, 262-269.
Verkleij, A. (1984) *Biochim. Biophys. Acta 779*, 43-63.
Verkleij, A. J., Van Echeld, G. J. A., Gerritsen, W. J., Cullis, P. R., & DeKruijff, B. (1980) *Biochim. Biophys. Acta 600*, 620-624.
Verkleij, A. J., De Maagd, R., Leunissen-Bijvelt, J., & DeKruijff, B. (1982) *Biochim. Biophys. Acta 684*, 255-262.
Weislander, A., Christiansson, A., Rilfors, L., & Lindblom, G. (1980) *Biochemistry 19*, 3650-3655.
Wilkinson, D. A., & Nagle, J. F. (1982) *Biochim. Biophys. Acta 688*, 107-115.
Wu, E. S., Jacobson, K., & Papahadjopoulos, D. (1977) *Biochemistry 16*, 3936-3941.
Yager, P., & Peticolas, W. L. (1982) *Biochim. Biophys. Acta 688*, 775-785.
Yager, P., & Chang, E. L. (1983) *Biochim. Biophys. Acta 731*, 491-494.

Deuterium NMR Investigation of Ether- and Ester-Linked Phosphatidylcholine Bilayers†

M. J. Ruocco, A. Makriyannis,‡ D. J. Siminovitch, and R. G. Griffin*
Francis Bitter National Magnet Laboratory, Massachusetts Institute of Technology, Cambridge, Massachusetts 02139
Received December 20, 1984

ABSTRACT: Deuterium nuclear magnetic resonance (^{2}H NMR) spectra of specifically head-group- and chain-deuterated ester- and ether-linked phosphatidylcholine bilayers were studied as a function of temperature over the range −33 to 50 °C. Head-group-deuterated dihexadecylphosphatidylcholine ([α-$^2H_2$]DHPC) bilayers yield line shapes and spin–lattice relaxation times similar to those observed for its ester-linked counterpart, dipalmitoylphosphatidylcholine ([α-$^2H_2$]DPPC), in the high-temperature ripple and L_α bilayer phases. These results indicate the ether linkage has no effect on the dynamics or the orientational order at the α-C^2H_2 segment of the phosphocholine head group. At all temperatures, the ^{2}H NMR spectra of chain-deuterated 1,2[1′,1′-$^2H_2$]DHPC bilayers exhibit a reduced spectral width compared to 1,2[2′,2′-$^2H_2$]DPPC bilayers. The most *significant* feature of the deuterated alkyl chain spectrum of DHPC at 45 °C is the observation of *four* separate quadrupolar splittings from the α-methylene segments of the alkyl chains, in comparison to the *three* quadrupolar splittings reported previously from the α-methylene segments of the acyl chains of DPPC. Spin–lattice relaxation experiments performed on DHPC suggest an assignment of the two smaller and the two larger quadrupolar splittings to separate alkyl chains, respectively. Low-temperature ($T \leq -20$ °C) gel-phase spectra of deuterated head-group [α-$^2H_2$]DHPC remain an order of magnitude narrower than those observed for [α-$^2H_2$]DPPC. Line shapes of chain-labeled DHPC are invariant to temperature over the 40 °C range from 20 to −20 °C, whereas in DPPC, there is a substantial change in the line shape below 0 °C. These observations may be explained by the formation of an interdigitated DHPC bilayer gel phase in which axial diffusion of the lipid molecule persists down to temperatures at least 20 °C below the temperature at which axial diffusion of DPPC ceases ($T \sim -7$ °C).

Deuterium nuclear magnetic resonance (^{2}H NMR)[1] of lipids containing deuterated acyl chains has become the method of choice for the determination of molecular conformation and dynamics within the lipid bilayer of model and biological membranes (Seelig, 1977; Seelig & Seelig, 1980; Jacobs & Oldfield, 1981; Griffin, 1981; Davis, 1983). With the exception of the sphingolipids, such as cerebrosides (Huang et al., 1980; Skarjune & Oldfield, 1979, 1982) and sphingo-

† This research was supported by the National Institutes of Health (GM-25505, GM-23289, and RR-00995) and by the National Science Foundation through its support of the Francis Bitter National Magnet Laboratory (DMR-8211416). D.J.S. and M.J.R. are recipients of postdoctoral fellowships from the Natural Sciences and Engineering Research Council of Canada and the National Multiple Sclerosis Society (FG291-A-1), respectively.
‡ On sabbatical leave from the School of Pharmacy and Institute of Materials Science, University of Connecticut, Storrs, CT 06268.

[1] Abbreviations: PC, phosphatidylcholine; ^{2}H NMR, deuterium nuclear magnetic resonance; DHPC, 1,2-dihexadecyl-*sn*-glycero-3-phosphocholine; DPPC, 1,2-dipalmitoyl-*sn*-glycero-3-phosphocholine; PE, phosphatidylethanolamine; PG, phosphatidylglycerol; PS, phosphatidylserine; DSC, differential scanning calorimetry; PA, phosphatidic acid; TLC, thin-layer chromatography; THF, tetrahydrofuran; TPS, 2,4,6-triisopropylbenzenesulfonyl chloride; [$^2H_{62}$]DPPC, 1,2-bis(perdeuteriopalmitoyl)-*sn*-glycero-3-phosphocholine.

0006-2960/85/0424-4844$01.50/0